MEASURING IN SITU ^{26}Al AND ^{10}Be IN POST-GLACIAL SAND REVEALS LIMITED EROSION BY QUEBEC-LABRADOR ICE DOME

A Thesis Presented

by

Peyton M. Cavnar

to

The Faculty of the Graduate College

of

The University of Vermont

In Partial Fulfillment of the Requirements
for the Degree of Master of Science in Natural Resources
Specializing in Arctic Climate Change

August 2024

Defense Date: May 14, 2024
Thesis Committee:

Paul R. Bierman, Ph.D., Advisor
John Crock, Ph.D., Chairperson
Jeremy D. Shakun, Ph.D.
Gillian Galford, Ph.D.
Holger Hoock, DPhil., Dean of the Graduate College

Abstract

There is minimal knowledge of the Laurentide Ice Sheet's erosive behavior prior to the Last Glacial Maximum because, as the ice sheet advanced, it largely erased evidence of previous glaciations. Seeking to understand the erosivity of the eastern portion of the Laurentide Ice Sheet, the Quebec-Labrador Ice Dome, we sampled sand from deglacial features (eskers and deltas) and from rivers across eastern Canada—a landscape repeatedly overrun by ice. We measured concentrations of ^{10}Be and ^{26}Al in quartz isolated from the sediment and, after considering cosmic ray exposure during the Holocene, used the data to determine nuclide concentration at the time of deglaciation. The mean ^{10}Be concentration in deglacial sediments (n=11) is 1.87 ±1.39*10^4 atoms/g and 3.31±1.57*10^4 atoms/g in modern sediments (n=10). Corrected for Holocene exposure, we determine that at the time it was deposited by the ice sheet, deglacial sediment contained between 7.60*10^3 and 5.58*10^4 atoms/g of ^{10}Be inherited from prior periods of surface and near-surface exposure. ^{26}Al/^{10}Be ratios corrected for Holocene nuclide production range from 3.45(- 2.26, + 1.10) to 8.45±4.19 in deglacial samples and 5.64±0.78 to 7.92±0.93 in modern river samples. Our data indicate that glacial erosion in eastern Canada was insufficient to remove cosmogenic nuclides produced during prior periods of exposure. This provides further evidence that the Laurentide Ice Sheet was minimally erosive during the last glacial period, as studies on other portions of the ice sheet also show inherited nuclide concentrations preserved by limited erosion. Most ^{26}Al/^{10}Be ratios for deglacial samples are near the production ratio for high latitudes, giving a strong indication that the Quebec-Labrador Ice Dome went through multiple periods of Pleistocene interglacial exposure.

Table of Contents

List of Tables

CHAPTER 2: JOURNAL ARTICLE

List of Figures

CHAPTER 2: JOURNAL ARTICLE

Chapter 1. Research Justification

During the last ice age, the Laurentide Ice Sheet (LIS) was a major influence on global climate and sea level (Gregoire et al., 2018). However, our knowledge of its erosivity and behavior (how persistent it was during interglacials and which portions deglaciated last) is limited to the last glacial maximum (LGM). In eastern Canada, the Quebec-Labrador Ice Dome (located around modern day Labrador City) is modeled as an epicenter for mass accumulation and distribution to other parts of the ice sheet that persisted through multiple glacial periods (Ullman, 2023; Stokes et al., 2012; Roy et al., 2009). There is evidence suggesting that it was one of the last areas of the LIS to deglaciate towards the end of the LGM (Dalton et al., 2020; Coutte et al., 2023). Aside from ice sheet modeling, research on the Quebec-Labrador Ice Dome is limited to a few studies dating glacial erratics and moraine systems using single nuclide exposure (Ullman et al., 2016; Couette et al., 2023).

Our study utilizes paired analysis of two cosmogenic nuclides, ^{26}Al and ^{10}Be, whose differing half lives cause $^{26}Al/^{10}Be$ ratios to reflect exposure and burial history over multiple glacial and interglacial cycles (Nishiizumi et al., 1991; Bierman et al., 1999). ^{26}Al and ^{10}Be concentrations in deglacial sediments allow us to analyze the burial history of sediments deposited out from under the LIS during deglaciation (Bierman et al., 1999; Nelson et al., 2014). Sampling along a transect of Quebec-Labrador that was under ice ~8 ka provides data on spatial variability of nuclide concentrations during the final retreat and disappearance of the Quebec-Labrador Ice Dome. We also performed $^{26}Al/^{10}Be$ analysis on modern river sediment as a comparison to sediments we assumed were buried under ice until the Holocene.

This data has the potential to justify or disprove models of how the Quebec-Labrador Ice Dome behaved throughout the Pleistocene, with $^{26}Al/^{10}Be$ ratios providing evidence of how erosive the ice dome was, and in conjunction, its basal thermal state (Melanson et al., 2013; Marshall et al., 2000). If the ratios are depressed (~4.5), this implies long term burial even during Pleistocene interglacials, corroborating the evidence found in LeBlanc et al.'s (2023) low-ratio ice rafted debris (IRD) suspected to have sourced from Quebec-Labrador. Further investigating how persistent the Quebec-Labrador Ice Dome was during interglacials will allow for more accurate modeling of ice sheet processes, applying to modern day studies of the Greenland Ice Sheet and Antarctica.

References

Bierman, P. R., Marsella, K. A., Patterson, C. J., Davis, P. T., & Caffee, M. W. (1999). Mid-Pleistocene cosmogenic minimum-age limits for pre-Wisconsinan glacial surfaces in southwestern Minnesota and southern Baffin Island: a multiple nuclide approach. *Geomorphology*, *27*(1–2), 25–39. https://doi.org/10.1016/s0169-555x(98)00088-9

Couette, P., Ghienne, J., Lajeunesse, P., & Woerd, J. (2023). Climatic control on the retreat of the Laurentide Ice Sheet margin in easternmost Québec–Labrador (Canada) revealed by cosmogenic nuclide exposure dating. *Journal of Quaternary Science, 38*(7), 1044-1061. https://doi.org/10.1002/jqs.3525

Dalton, A., Margold, M., Stokes, C., Tarasov, L., Dyke, A. S., Adams, R. S., Allard, S., Atends, H. E., Atkinson, N., Attig, J. W., Barnett, P., Barnett, R., Batterson, M., Bernatchez, P., Borns, H. W., Breckenridge, A., Briner, J. P., Brouard, E., Campbell, J. E., Carlson, A. E.,..., Wright, H. E. (2020). An Updated Radiocarbon-Based Ice Margin Chronology for the Last Deglaciation of the North American Ice Sheet Complex. *Quaternary Science Reviews, 234*(15), 0277-3791. https://doi.org/10.1016/j.quascirev.2020.106223

Gregoire, L., Ivanović, R., Maycock, A. C., Valdes, P. J., & Stevenson, S. (2018). Holocene lowering of the Laurentide ice sheet affects North Atlantic gyre circulation and climate. *Climate Dynamics*, *51* (9–10), 3797–3813. https://doi.org/10.1007/s00382-018-4111-9

LeBlanc, D. E., Shakun, J. D., Corbett, L. B., Bierman, P. R., Caffe, M. W., & Hidy, A. J. (2023). Laurentide Ice Sheet Persistence During Pleistocene Interglacials. *Geology, 51*(5), 496-499. https://doi.org/10.1130/G50820.1

Marshall, S. J., Tarasov, L., Clarke, G. K. C., & Peltier, W. R. (2000). Glaciological reconstruction of the Laurentide Ice Sheet: physical processes and modelling challenges. *Canadian Journal of Earth Sciences*, *37*(5), 769–793. https://doi.org/10.1139/e99-113

Melanson, A., Bell, T., & Tarasov, L. (2013). Numerical modelling of subglacial erosion and sediment transport and its application to the North American ice sheets over the Last Glacial cycle. *Quaternary Science Reviews*, *68*, 154–174. https://doi.org/10.1016/j.quascirev.2013.02.017

Nelson, A. H., Bierman, P. R., Shakun, J. D., & Hood, D. H. (2014). Using in situ cosmogenic 10Be to identify the source of sediment leaving Greenland. *Earth Surface Processes and Landforms, 39*, 1087-1100. 10.1002/esp.3565

Nishiizumi, K., Kohl, C. P., Arnold, J. R., Klein, J., Fink, D., & Middleton, R. (1991). Cosmic ray produced 10Be and 26Al in Antarctic rocks: exposure and erosion history. *Earth and Planetary Science Letters*, *104*(2–4), 440–454. https://doi.org/10.1016/0012-821x(91)90221-3

Roy, M., Hemming, S. R., & Parent, M. (2009). Sediment sources of northern Québec and Labrador glacial deposits and the northeastern sector of the Laurentide Ice Sheet during ice-rafting events of the last glacial cycle. *Quaternary Science Reviews*, *28*(27–28), 3236–3245. https://doi.org/10.1016/j.quascirev.2009.08.008

Ullman, D. (2023). The retreat chronology of the Laurentide Ice Sheet during the last 10,000 years and implications for deglacial sea-level rise. *Vignettes: Key Concepts in Geomorphology.* https://serc.carleton.edu/59463.

Ullman, D., Carlson, A. E., Hostetler, S. W., Clark, P. U., Cuzzone, J., Milne, G. A., Windsor, K., & Caffe, M. (2016). Final Laurentide ice-sheet deglaciation and Holocene climate-sea level change. *Quaternary Science Reviews, 152*(15), 49.59. https://doi.org/10.1016/j.quascirev.2016.09.014

Measuring in situ ^{26}Al and ^{10}Be in Post-Glacial Sand Reveals Limited Erosion by Quebec-Labrador Ice Dome*

* Manuscript to be submitted to *Geochronology*

Peyton M. Cavnar[1,2], Paul R. Bierman[1,2], Jeremy D. Shakun[3], Lee B. Corbett[1,2], Danielle LeBlanc[3], Gillian Galford[1,2], and Marc Caffee[4]

[1]Rubenstein School for the Environment and Natural Resources, University of Vermont, Burlington, 05405, United States

[2]Gund Institute for the Environment, Burlington, 05405, United States

[3]Morrissey College of Arts and Sciences, Boston College, Chestnut Hill, 02467, United States

[4]PRIME Laboratory, Purdue University, West Lafayette, 47907, United States

Correspondence to: Peyton M. Cavnar (cavnar.peyton@gmail.com)

Abstract. There is minimal knowledge of the Laurentide Ice Sheet's erosive behavior prior to the Last Glacial Maximum because, as the ice sheet advanced, it largely erased evidence of previous glaciations. Seeking to understand the erosivity of the eastern portion of the Laurentide Ice Sheet, the Quebec-Labrador Ice Dome, we sampled sand from deglacial features (eskers and deltas) and from rivers across eastern Canada—a landscape repeatedly overrun by ice. We measured concentrations of ^{10}Be and ^{26}Al in quartz isolated from the sediment and, after considering cosmic-ray exposure during the Holocene, used the data to determine nuclide concentration at the time of deglaciation. The mean ^{10}Be concentration in deglacial sediments (n=11) is 1.87 ±1.39*10^4 atoms g^{-1} and 3.31±1.57*10^4 atoms g^{-1} in modern sediments (n=10). Corrected for Holocene exposure, we determine that deglacial sediment, at the time it was deposited by the ice sheet, contained between 7.60*10^3 and 5.58*10^4 atoms g^{-1} of ^{10}Be inherited from prior periods of surface and near-surface exposure. $^{26}Al/^{10}Be$ ratios corrected for Holocene nuclide production range from 3.45(-2.26, + 1.10) to 8.45±4.19 in deglacial samples and 5.64±0.78 to 7.92±0.93 in modern river samples. Our data indicate that glacial erosion in eastern Canada was insufficient to remove cosmogenic nuclides produced during prior periods of exposure. This provides further evidence that the Laurentide Ice Sheet was minimally erosive during the last glacial period, as studies on other portions of the ice sheet also show inherited nuclide concentrations preserved by limited erosion. Most $^{26}Al/^{10}Be$ ratios for deglacial samples are near the production rate for high latitudes, giving a strong indication that the Quebec-Labrador Ice Dome went through multiple periods of Pleistocene interglacial exposure.

1. Introduction

During the Last Glacial Maximum (LGM), about 20-25,000 years ago, more than half of the continental Northern Hemisphere was covered by ice (Ullman, 2023). The Laurentide Ice Sheet (LIS) was then the most expansive body of ice in the Northern Hemisphere. At its peak, the LIS covered most of Canada and advanced southward into the northern United States (Munroe et al., 2016; Margold et al., 2018;

Dalton et al., 2020). The LIS influenced global climate, atmospheric circulation, ocean currents, and sea level (Gregoire et al., 2018). Its disappearance during the latest Pleistocene and early Holocene (characterized by collapse of northern Canadian ice domes) revealed a complicated paraglacial landscape: one in which cycles of advance and retreat left behind deglacial landforms while destroying those created previously (Occhietti et al., 2011). Because of this, it is difficult to ascertain from the landscape much about LIS behavior prior to the LGM. While marine sediment cores may record millions years of history, tracing the provenance of marine sediment to a specific region of the ice sheet with certainty is often a challenge (Roy et al., 2009; LeBlanc et al., 2023).

Using cosmogenic nuclides to date and understand paleo ice sheet behavior is a relatively recent approach, with the first studies taking place in the 1980s (Blanckenburg & Willenbring, 2014; Nishiizumi et al., 1989; Gosse & Phillips, 2001; Staiger et al., 2005). Cosmogenic nuclides are rare isotopes created when cosmic radiation from the galaxy bombards Earth and its atmosphere (Gosse & Phillips, 2001). The high-energy cosmic rays collide with atoms in the atmosphere, creating secondary neutrons through spallation. Spallation-induced neutrons that fall to Earth's surface (and a few meters below it) create *in situ* (in the position of collision) cosmogenic nuclides such as ^{26}Al and ^{10}Be in minerals including weathering-resistant quartz (Schaefer et al., 2022). Smaller particles, muons, are also created during atmospheric interactions with cosmic rays (Dunai & Lifton, 2014). However, since muons have very low reactivity with matter, they are able to penetrate far more deeply into the Earth's surface than neutrons (Braucher et al., 2011). At depths below 2 meters, muons are responsible for the majority of subsurface production of cosmogenic nuclides (Braucher et al., 2003).

Rates and dates of landscape change can be measured using only one cosmogenic nuclide (Bierman, 1994). However, a dual isotope approach allows for a more detailed understanding of glacial behavior over time because of the different decay rates of ^{10}Be (half-life ~1.36 My) and ^{26}Al (half-life ~730 ky) (Nishiizumi et al., 2007; Nishiizumi, 2004; Nishiizumi et al., 1991; Bierman et al., 1999). When exposed to cosmic radiation in polar regions, *in situ* ratios of ^{26}Al/^{10}Be at production are 7.3±0.3 (1σ) (Corbett et al., 2017). When a landform is covered by a thick layer of ice such as the LIS, it is shielded from cosmic radiation. This stops the production of *in situ* ^{26}Al and ^{10}Be. As isotopes produced during initial exposure decay, the ^{26}Al/^{10}Be ratio falls (Klein et al., 1986; Bierman et al., 1999). Despite Holocene exposure to cosmic rays following LIS retreat, ^{26}Al/^{10}Be ratios depressed by LIS cover for geologically significant time periods (10^5 to 10^6 y) can be preserved if this sediment is buried meters below the surface (such as in deglacial deltas, coastal bluffs, or eskers) (Corbett et al., 2016b). Modern river sediment, if it is sourced closer to the surface, will have higher concentrations of *in situ* ^{26}Al and ^{10}Be and a higher ^{26}Al/^{10}Be ratio because of recent exposure to cosmic radiation.

In this paper, we present concentrations of ^{26}Al and ^{10}Be measured in quartz isolated from deglacial and modern river sediments in Labrador and Quebec, Canada. After correcting deglacial concentrations for Holocene nuclide production, we use these data and the ^{26}Al/^{10}Be ratio to infer paleo ice sheet coverage and the LIS's erosion efficiency during the Pleistocene. The results allow us to infer LIS

persistence and erosivity throughout the Pleistocene, improve interpretation of cosmogenic analysis of glacially derived sediment in marine sediment cores, and provide an analog for the behavior of modern ice sheets including the current deglaciation of Greenland.

2. Background

As the LIS grew to its greatest extent during the LGM, it bulldozed most moraines, eskers, and other landforms created during lesser LIS extents (Dyke, 2004). Because of this, few terrestrial records remain of LIS pre-LGM behavior. In Quebec and Labrador, abundant rounded bedrock outcrops provide evidence for a once erosive LIS with warm-based, fast-sliding ice (Roy et al., 2009). Simultaneously, the presence of multiple sets of striations on glacially eroded bedrock in this region suggests that the LIS was also once cold-based, allowing the preservation of such features (Kleman et al., 1994; Roy et al., 2009). Because the advancing LIS destroyed evidence of its past margins and we cannot determine if these striations are from the most recent glaciation or preserved from ones prior, our knowledge about how erosive or extensive the LIS was prior to the LGM is limited (Batchelor et al., 2019). However, because the cosmogenic nuclides ^{10}Be and ^{26}Al are preserved in both rock and buried deglacial sediment, measuring their concentrations allows researchers to circumvent the limitations of traditional terrestrial records and determine the depth of glacial erosion and set limits on the extent and timing of burial by ice sheets (Briner et al., 2016; Bierman et al., 2016; Marsella et al., 2000; Corbett et al., 2016b; Stroeven et al., 2002; Staiger et al., 2006; Harbor et al., 2006).

2.1 Laurentide Ice Sheet History and Deglaciation

For the majority of its most recent inception (~118 ka) to final deglaciation (~8 ka), the LIS was characterized three major ice domes, regions of especially thick ice (~4 km in some places) that accumulated and dispersed mass (Ullman, 2023; Stokes et al., 2012; Roy et al., 2009). Ensemble ice modeling supports the formation of the Foxe Baffin Dome first (~118 ka), with ice growth then progressing southward to create the Keewatin Dome (~116 ka), and later the nucleus of the Quebec-Labrador Ice Dome (~114 ka) (Stokes et al., 2012). The majority of Canada was covered by Marine Oxygen Isotope (MIS) stage 5d (~110 ka), with ice cover being 80% of what it would be during the LGM (Stokes et al., 2012). From 120-70 ka, the LIS alternated from being made up of three unconnected domes to one body of ice (Stokes et al., 2012; Kleman et al., 2010).

There is debate over how extensive and persistent the LIS was during Pleistocene interglacials (Pico et al., 2018; LeBlanc et al. 2023; Miller & Andrews, 2019; Batchelor et al., 2019; Dalton et al., 2019). Cosmogenic nuclides (^{26}Al and ^{10}Be) in ice-rafted debris (IRD) from LIS discharge during the last glacial period have been used to infer the burial and exposure history of glacial sediment prior to its transport to the ocean (LeBlanc et al., 2023). These IRD samples had ^{26}Al/^{10}Be ratios ~4, substantially lower than at production, suggesting long periods of burial by ice throughout the Pleistocene, as interglacials with little to no ice would have yielded IRD with higher ratios (LeBlanc et al., 2023). LeBlanc

et al.'s (2023) cosmogenic data challenge the commonly held assumption that all Pleistocene interglacials resulted in fully ice-free conditions for at least thousands of years.

A similar debate concerns the magnitude of LIS retreat during interstadials within the last glacial period. A combination of luminescence dating, ^{14}C dating, and cosmogenic nuclides (^{26}Al and ^{10}Be), along with evidence of a marine incursion into Hudson Bay, suggest that the portion of the LIS over Hudson Bay deglaciated during MIS 3 (Dalton et al., 2019). However, the reliability of these ages has been questioned (Miller & Andrews, 2019) and the timing of carbonate-rich Heinrich events H5 and H4 suggest that an intact Hudson Strait ice stream existed during MIS 3. With this debate unsettled, it remains uncertain how much the LIS retracted during interstadial periods.

Further studies have investigated LIS sensitivity to climate shifts that led to the collapse of the Quebec-Labrador Ice Dome. There is evidence for close ties between regional deglaciation and climate fluctuations based on dating of 37 bedrock samples collected throughout Quebec and Labrador (Couette et al., 2023). These data reveal five still-stands or re-advances of the eastern LIS margin (~12.9 ka, ~11.5 ka, ~10.4 ka, ~9.3 ka, and ~8.4-8.2 ka) before its final collapse (Couette et al., 2023). These periods correspond temporally with GrIS marine core layers rich in IRD, likely brought about by early Holocene abrupt cooling events (Couette et al., 2023). The data also suggest that the Quebec-Labrador Ice Dome was sustained during the early Holocene because of localized cooling from meltwater discharge during these periods of retreat stagnation (Couette et al, 2023). Furthermore, final deglaciation of the Quebec Labrador Ice Dome lagged ~4 ka behind peak Holocene insolation and CO_2 forcing (Ullman et al., 2016), making it one of the longest lasting portions of the LIS after the LGM (Ullman, 2023).

2.2 Sediment Sourcing From Ice Sheets and Deglacial Landscapes

Cosmogenic isotopes have been used to identify sediment sources for both modern and paleo ice sheets (Nelson et al., 2014; Corbett et al., 2021; Goehring et al., 2010; Bierman et al., 2016). ^{10}Be isolated from quartz in glacial, deglacial, and mixed terrain in Greenland showed no statistically significant difference ($P = 0.64$) between sediment sourced from glacial terrain and that sourced from a mix of deglaciated and glaciated areas. The mean ^{10}Be concentration in deglacial terrain was significantly greater than means of the other two groups ($P < 0.0001$) (Nelson et al., 2014). This is explained by the non-glacial sediment having been exposed to cosmic radiation since Holocene deglaciation (Nelson et al., 2014). Because the ^{10}Be concentration in the mixed terrain samples (glacial-fluvial and terrace) is low (~5.5 ± $2.2*10^3$ atoms/gram) like that from the deglacial terrain, it indicates that both deglacial and river sediments originated from under the GrIS where production of ^{10}Be is minimal (Nelson et al., 2014). Therefore, the majority of sediment on glacial and paraglacial landscapes in Greenland comes from the under glacier opposed to the adjacent deglaciated areas (Nelson et al., 2014).

In southwest Minnesota and eastern South Dakota, a similar approach was used to determine sediment sourcing from a deglaciated part of the midwestern United States, where ice has not been present since the final retreat of the LIS (Balco et al., 2005). After analyzing $^{26}Al/^{10}Be$ concentrations in modern

river sand, Balco et al. determined that Wisconsinan glacial sediment and outwash and modern Minnesota River sediment had nearly identical concentrations of both nuclides (Balco et al., 2005). If the modern sediment were coming from the nearby, slowly eroding, exposed soil sources, it would have a significantly higher concentration of nuclides compared to deglacial sediment both outwash and till (Balco et al., 2005). These data suggest that in at least some paraglacial landscapes, both modern and deglacial river sediments are all sourced primarily from the rapid erosion of steep river cutbacks that expose glacial deposits. The data of Balco et al. suggest that ^{26}Al and ^{10}Be concentrations can distinguish the source of fluvial sediments in previously glaciated terrain.

2.3 Assessing the Erosivity of Ice Sheets

Isolating ^{10}Be from bedrock and glacial erratics within the historical range of the Quebec-Labrador Ice Dome reveals a pattern of deep erosion in some places and in others, evidence for inherited ^{10}Be and minimal subglacial erosion (Couette et al, 2023; Ullman et al., 2016). Boulders sampled from the Paradise Moraine system (once the ice dome's coastal margin) have unusually high concentrations of ^{10}Be (Couette et al, 2023; Ullman et al., 2016). One study had two samples dated >20 ka from this system, while later sampling revealed an average ^{10}Be concentration of ~85600 (atoms g^{-1}), with 4 out of 6 samples inaccurately dating the moraine as being older than a margin further east (Couette et al, 2023; Ullman et al., 2016). Boulder recycling and inheritance of nuclides from prior periods of near-surface exposure explain these unusually high concentrations of ^{10}Be (Couette et al, 2023; Ullman et al., 2016). In this scenario, a minimally erosive LIS would allow the preservation of ^{10}Be and ^{26}Al concentrations on previously exposed boulders plucked from bedrock surfaces that were not deeply eroded by ice.

Similar methods were used to assess the erosivity of the Greenland Ice Sheet by measuring ^{10}Be, ^{26}Al, and ^{14}C in subglacial cobbles (n = 86) transported to the western ice margin (Corbett et al., 2021). Most cobbles had a very low (median $1.0*10^3$ atoms/gram) concentration of ^{10}Be, indicative of deep subglacial erosion and/or minimal prior surface exposure time (Corbett et al., 2021). The large sample size and assumed path of transport to the margin via ice and/or meltwater supports the assumption that western GrIS is mostly characterized by deep subglacial erosion (Corbett et al., 2021). These samples' $^{14}C/^{10}Be$ ratios of ~6 suggest that much of the recent nuclide production is due to muons while the sediment was shielded (either by bedrock or a consistent thin layer of ice) (Corbett et al., 2021). The glacially sourced cobbles with nuclide concentrations suggest little to no inheritance of nuclides from prior exposure periods (Corbett et al., 2021). A subset of samples with high ^{10}Be concentrations ($> 3*10^3$) includes both subglacial cobbles (n=14) and proglacial cobbles (n=9) (Corbett et al., 2021). The subglacial cobbles with high ^{10}Be appear to be sourced from regions near the ice margin that were likely cold-based and minimally erosive (Corbett et al., 2021). This would create pockets of non-eroded bedrock where accumulated ^{10}Be from prior exposures (MIS5e or earlier) could be preserved (Corbett et al., 2021).

In Norway, glacial erratic boulders were sampled at depth (>2.5 m) on the island of Utsira, once near the margin of the Scandinavian Ice Sheet (Briner et al., 2016). ^{10}Be concentrations of the samples

(n=7) corresponded to ages that were >10% too old (~20 ka) for an island on the periphery of the Scandinavian Ice Sheet, only being covered by ice during maximum phases of glaciation (Briner et al., 2016). The relatively uniform concentration of inherited ^{10}Be among all samples suggests that nuclide concentrations are the product of muon-induced production at depth (Briner et al., 2016). Assuming brief glaciations during only maximum glacial phases, long exposure time at Utsira boulders coupled with ineffective glacial erosion would preserve this muonogenic and now inherited ^{10}Be. Glacial erosion > 5 m deep would be needed to lower inherited ^{10}Be concentrations to undetectable quantities (Briner et al., 2016). Because Utsira is an island, it is assumed that the boulders are locally sourced instead of the product of boulder recycling, providing more evidence of insufficient erosion endemic to the southwest margin of the Scandinavian Ice Sheet (Briner et al., 2016).

3. Setting

The Quebec-Labrador Ice Dome occupied the eastern subarctic Canadian Shield, where bedrock consists of mostly Proterozoic quartzofeldspathic gneisses and granites (Hynes & Rivers, 2010). Because of the region's glacial history, soils are thin, allowing for prominent bedrock outcrops and large glacial erratics (Ullman et al., 2016). Central/southern Quebec-Labrador also includes multiple moraine systems that track the final deglaciation of the ice dome into the early Holocene (Ullman et al. 2016). The paraglacial landscape is currently experiencing isostatic glacial rebound, with changes in elevation since deglaciation being more prominent towards the past location of the center of the dome (Andrews & Tyler, 2011). Prominent isostatic rebound occurred near James Bay and southern Hudson Bay, with ~300 m of recorded rebound compared to ~100 m along the coastal northwestern margin (Andrews & Tyler, 2011).

Notable geographic features of this region include the St. Lawrence River, the Churchill River, and the Manicouagan Reservoir, an annular lake north of the St. Lawrence gulf formed in a depression caused by a meteor impact (Spray et al., 1998). The St. Lawrence River flows from southwest to northeast into the Gulf of St. Lawrence and is located southeast of the dome's center (Süfke et al., 2022). During LIS's final deglaciation, the St. Lawrence River served as one of the major meltwater drainage systems (Süfke et al., 2022). The Churchill River flows east and towards the coast near one of the dome's last places to deglaciate, draining into Lake Melville and then the Atlantic Ocean (Canadian Geographic, n.d.).

The ecology of eastern Canada is dominated by boreal spruce forests, sedges, and muskegs (shallow bogs covered in moss) (Payette et al., 1989). This sub-arctic ecosystem is prone to burning during abnormally arid periods in the summer, with a recorded fire history stretching back to the 1950's (Payette et al., 1989). Northern Quebec and Labrador is classified under the Dfc climate zone (cool continental climate/subarctic) according to the Koppen climate classification system (Amani et al., 2019; Beck et al., 2018). In winter, ground based measurements record a mean of ~158 mm of snow water equivalent (SWE) for eastern Canadian boreal forests (Larue et al., 2017).

4. Methods

4.1 Field Methods

Starting in Goose Bay, Labrador, we sampled northeast to southwest across the former area of the ice dome (Figure 1). We chose sample sites based on proximity to the Trans-Labrador Highway and Route 389. We sampled deglacial landforms (n=11) including ice-contact deltas, eskers, and glacially-molded bedrock to constrain nuclide concentrations in materials directly affected by the ice sheet (Table 1). We took sediment from deltas and eskers on clean faces in gravel pits from 2 to 30 meters below the upper surface to ensure minimal nuclide production following deglaciation. We used shovels to dig ~0.3 meters into the side of the landform before collecting ~500 grams of sand. We collected one bedrock sample (~800 grams) to provide insight into inherited nuclides remaining in rock from prior periods of exposure (Table 1). We also collected modern river sediment samples (n=10) from main river trunks as well as smaller tributaries to compare their ^{10}Be concentration and ^{26}Al/^{10}Be ratios to those of deglacial samples (Table 1). When taking from sandbars with a substantial amount of pebbles and cobbles, we wet sieved samples between 250-850 micrometers during collection.

Table 1. Sample Location and Type

Sample Name	Type[a]	Latitude[b]	Longitude[b]	Sample Site Elevation (m)[b]
CF-02	Deglacial Sediment	53.5077	-63.9545	167
LC-02	Deglacial Sediment	52.2011	-67.8722	537
LC-04	Deglacial Sediment	51.7102	-68.0719	440
LC-05	Deglacial Sediment	51.4881	-68.2192	391
MC-01	Deglacial Sediment	50.4748	-68.8101	500
MC-02	Deglacial Sediment	48.6452	-69.0854	10
GB-03	Deglacial Sediment	53.2572	-60.3135	36
GB-05	Deglacial Sediment	53.0922	-61.8920	402
SS-01	Deglacial Sediment	48.1030	-69.7213	10
SS-05	Deglacial Sediment	47.1669	-70.8047	307
CF-01	Modern River Sediment	53.5060	-63.9585	126

CF-05	Modern River Sediment	53.0595	-66.2555	527
LC-01	Modern River Sediment	52.3365	-67.5671	533
LC-03	Modern River Sediment	52.1107	-68.0073	645
LC-06	Modern River Sediment	51.4882	-68.2229	401
GB-02	Modern River Sediment	53.3934	-60.4229	1.52
GB-04	Modern River Sediment	53.2201	-60.9549	210
MC-03	Modern River Sediment	48.6779	-69.3045	61
SS-02	Modern River Sediment	47.8942	-69.9368	128
SS-03	Modern River Sediment	47.6665	-70.1589	3
SS-04	Modern River Sediment	47.5157	-70.5066	25
GB-06	Bedrock	53.3351	-62.9912	484

[a] Deglacial sediment is sand that was deposited from the LIS as it was retreating, often found in deglacial landforms like eskers or coastal bluffs. Modern river sediment was collected from rivers and streams where we assumed surface exposure during the Holocene.

[b] Location and elevation were measured in the field using a Garmin eTrex 20 GPS

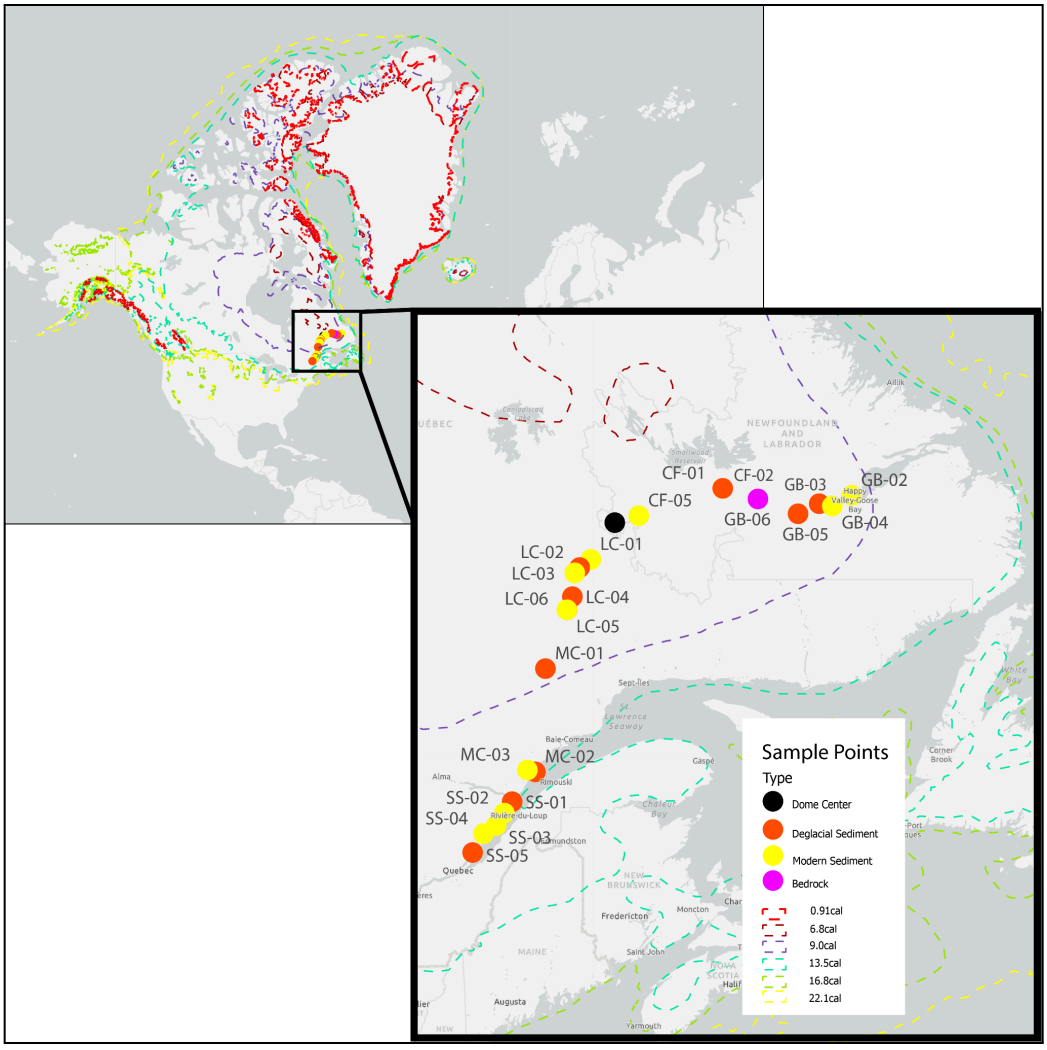

Figure 1. Field Area
Sampling locations are color coded by type. The black dot represents the center of the Quebec-Labrador Ice Dome, estimated to be where modern day Labrador City is (Couette et al., 2023). Dotted lines represent LIS margins provided from findings in Dalton et al,. 2020. Different colored lines each correspond to a calibrated age in ka (see legend).

4.2 Laboratory Methods

To isolate and purify quartz for cosmogenic nuclide analysis, we used a series of physical and chemical processes (Corbett et al., 2016a; Kohl & Nishiizumi, 1992). We mechanically sieved samples and saved material between 250-850 micrometers for further processing. With each sample, we performed two 24 hour 6 N hydrochloric acid etches in heated ultrasonic baths to remove grain coatings. We then used diluted (1%) hydrofluoric and nitric acid etches for three 24 hour periods after which we sonicated samples in 0.5% HF and HNO_3 for a minimum of two weeks (Corbett et al., 2016a; Kohl & Nishiizumi, 1992).

We tested the purity of etched samples using inductively coupled plasma spectrometry optical emission (ICP-OES) after which impure samples were re-etched until they were sufficiently pure. Pure

quartz samples (17.34-22.15 g) were extracted in the NSF/UVM Community Cosmogenic Facility clean lab. Anion and cation columns were used to remove unwanted elements such as titanium and magnesium, as well as to isolate aluminum and beryllium in each sample (Corbett et al., 2016a). After extraction, we sent ^{10}Be and ^{26}Al cathodes to PRIME Laboratory for analysis using accelerator mass spectrometry. Beryllium ratios were normalized against standard 07KNSTD3110 with an assumed ratio of 2850 x 10^{-15} (Nishiizumi et al., 2007). Aluminum ratios were normalized using standard KNSTD with an assumed ratio of 1.818 x 10^{-12} (Nishiizumi et al., 2004).

4.3 Data Reduction

We used the known concentration of ^{9}Be added as carrier, along with the measured isotopic ratio and quartz mass to calculate the concentration of ^{10}Be in each sample. Because of the native ^{27}Al within the samples, the concentration of ^{27}Al measured using ICP-OES after quartz dissolution was used to calculate the concentration of ^{26}Al. We subtracted the mean extraction process blank ratio of ^{10}Be/^{9}Be ($7.41\pm2.81*10^{-16}$; n=2) and ^{26}Al/^{27}Al ($5.39\pm0.71*10^{-16}$; n=2) from the measured ratios and propagated the uncertainty in quadrature (Table 2).

For deglacial (n =11) samples, we calculated how much nuclide production was attributable to Holocene exposure (Table 3). Using the CRONUS online exposure age calculator (constant production rate model, version 3.0.2, constants 2020-08-26), we calculated the production rate (atoms g^{-1} yr^{-1}) of ^{10}Be and ^{26}Al for both muons and spallation for each sample. This allowed us to calculate the production since deglaciation (atoms g^{-1}) of ^{10}Be and ^{26}Al at each sampling depth (Bierman, 1994). Thus, the amount of ^{10}Be or ^{26}Al (H in atoms g^{-1}) created post-deposition can be calculated by:

$$H = T_p \cdot A \quad (1)$$

$$T_p = D_\mu + D_s \quad (2)$$

Where T_p is the total production rate at sampling depth and A is the age of deglaciation for the sample site (yr). Deglaciation age estimates for each sample site are taken from Ullman et al. (2016) and Dalton et al. (2020). To calculate total production rate at sampling depth, we summed the production rate at the sampling depth for muons (D_μ) and spallation (D_s) obtained from CRONUS output for surface level muonic and spallation production. To calculate spallation production rates, we used a Λ of 165 g/cm^{-2}. A Λ value of 1400 g cm^{-2} was used for calculating muonogenic production rates since production rates lower more slowly with depth than do those from spallation. We calculated error for Holocene corrected samples by estimating a margin of uncertainty for individual sample depth (Table 3a). Inherited nuclide concentrations were calculated for the minimum and maximum estimated depth for each sample and were propagated with error in atoms g^{-1} from AMS data reduction.

To correct for Holocene exposure in our bedrock sample (GB-06), we used Ullman's et al., 2016 data to approximate the sample's age of deglaciation (7.6 ka, from Ullman et al.'s CL3 transect). Subtracting this age from our CRONUS output yielded an age difference of ~3200 years. Using the same procedure outlined above for calculating spallation and muonogenic production rates, we calculated the amount of ^{10}Be and ^{26}Al produced in ~3200 years as the estimated concentration of inherited nuclides.

5. Results

In situ produced cosmogenic ^{10}Be and ^{26}Al were present above detection limits in all 22 samples we analyzed (Table 2). Measured concentrations of ^{10}Be ranged from $8.42\pm1.68*10^3$ to $55.9\pm2.63*10^3$ atoms g^{-1} with a mean of $3.01*10^4$ and a median of $2.41*10^4$ atoms g^{-1}. Measured concentrations of ^{26}Al ranged from $2.78\pm2.65*10^4$ to $59.0\pm2.9*10^4$ atoms g^{-1} with a mean of $19.9*10^4$ and a median of $15.7*10^4$. Measured ratios of ^{26}Al/^{10}Be ranged from 4.89±0.60 to 8.44±4.19 with a mean of 6.49 and a median of 6.47. The single bedrock sample (GB-06) had a ^{10}Be concentration of $73.3\pm3.90*10^3$ atoms g^{-1} and a ^{26}Al concentration of $59.0\pm2.90*10^4$ atoms g^{-1}, and a ^{26}Al/^{10}Be ratio of 8.05±0.58. This is the sample with the highest measured concentration of ^{10}Be and ^{26}Al. Using the LSDn scaling scheme, this outcrop has an exposure age of 10,800±860 years (external error, 1 SD).

A Wilcoxon rank-sum test revealed that there is no significant difference between the measured mean concentrations of ^{10}Be for modern river sediment ($3.31\pm1.57*10^4$ atoms g^{-1}, n=11) and deglacial ($2.25\pm1.30*10^4$ atoms g^{-1}, n=10) sediment samples (alpha = 0.05, p = 0.11). Similarly, there is no significant difference between the mean concentrations of ^{26}Al for modern ($2.12\pm1.18*10^5$ atoms g^{-1}, n=11) and deglacial ($14.7\pm9.40*10^4$ atoms g^{-1}, n=10) samples (alpha = 0.05, p = 0.13). The concentrations of ^{10}Be and ^{26}Al in the bedrock sample are more than twice the mean concentration of each nuclide for both sample types.

Table 2a. Measured Isotopic Data for ^{10}Be

Sample Name	Type	Quartz Mass (g)	Be Carrier Solution Mass (g)	Uncorrected $^{10}Be/^{9}Be$ Ratio [a]	Uncorrected $^{10}Be/^{9}Be$ Ratio Uncertainty [a]	Background Corrected $^{10}Be/^{9}Be$ Ratio	Background Corrected $^{10}Be/^{9}Be$ Ratio Uncertainty	Measured ^{10}Be (atoms g^{-1})	^{10}Be Uncertainty (atoms g^{-1})	Cathode #
CF-02	Deglacial	20.46	0.7353	2.31E-14	1.55E-15	2.23E-14	1.58E-15	1.84E+04	1.30E+03	169432
LC-02	Deglacial	21.95	0.7364	3.11E-14	1.87E-15	3.04E-14	1.89E-15	2.34E+04	1.45E+03	169436
LC-04	Deglacial	19.74	0.7348	2.45E-14	1.54E-15	2.38E-14	1.57E-15	2.04E+04	1.34E+03	169438
LC-05	Deglacial	19.29	0.7348	3.26E-14	2.13E-15	3.18E-14	2.15E-15	2.79E+04	1.88E+03	169439
MC-01	Deglacial	19.60	0.7342	2.24E-14	1.85E-15	2.17E-14	1.88E-15	1.86E+04	1.61E+03	169441
MC-02	Deglacial	18.75	0.7319	2.16E-14	1.69E-15	2.09E-14	1.71E-15	1.87E+04	1.54E+03	169442
GB-03	Deglacial	9.38	0.7353	5.42E-15	8.92E-16	4.68E-15	9.35E-16	8.42E+03	1.68E+03	169444
GB-05	Deglacial	20.10	0.7310	2.70E-14	2.37E-15	2.62E-14	2.39E-15	2.19E+04	1.99E+03	169447
SS-01	Deglacial	19.70	0.7337	1.36E-14	1.48E-15	1.28E-14	1.50E-15	1.10E+04	1.29E+03	169450
SS-05	Deglacial	20.88	0.7308	7.02E-14	3.26E-15	6.95E-14	3.28E-15	5.59E+04	2.63E+03	169454
CF-01	Modern	18.52	0.7331	2.82E-14	2.37E-15	2.75E-14	2.39E-15	2.50E+04	2.17E+03	169431
CF-05	Modern	20.92	0.7348	6.55E-14	2.69E-15	6.48E-14	2.71E-15	5.23E+04	2.18E+03	169434
LC-01	Modern	20.41	0.7330	6.44E-14	2.81E-15	6.37E-14	2.83E-15	5.26E+04	2.33E+03	169435
LC-03	Modern	20.50	0.7307	6.88E-14	2.93E-15	6.81E-14	2.94E-15	5.58E+04	2.41E+03	169437
LC-06	Modern	19.44	0.7345	3.14E-14	2.42E-15	3.07E-14	2.44E-15	2.67E+04	2.12E+03	169440
GB-02	Modern	19.96	0.7311	1.75E-14	1.65E-15	1.68E-14	1.67E-15	1.41E+04	1.41E+03	169443
GB-04	Modern	17.34	0.7362	1.72E-14	1.39E-15	1.65E-14	1.42E-15	1.61E+04	1.39E+03	169445
MC-03	Modern	20.73	0.7304	2.51E-14	2.03E-15	2.44E-14	2.05E-15	1.98E+04	1.66E+03	169449
SS-02	Modern	20.37	0.7345	3.44E-14	2.41E-15	3.37E-14	2.43E-15	2.79E+04	2.01E+03	169451
SS-03	Modern	20.81	0.7349	3.31E-14	2.17E-15	3.24E-14	2.19E-15	2.63E+04	1.78E+03	169452

SS-04	Modern	22.15	0.7349	6.31E-14	2.82E-15	6.24E-14	2.83E-15	4.76E+04	2.16E+03	169453
GB-06	Bedrock	15.35	0.7365	6.73E-14	3.53E-15	6.65E-14	3.54E-15	7.33E+04	3.90E+03	169448

[a] Isotopic analysis conducted at PRIME Laboratory; ratios were normalized against standard 07KNSTD3110 with an assumed ratio of 2850 x 10^{-15} (Nishiizumi et al., 2007).

Table 2b. Measured Isotopic Data for ^{26}Al

Sample Name	Type	Quartz Mass (g)	Al Carrier Solution Mass (g)	Uncorrected ^{26}Al/^{27}Al Ratio [a]	Uncorrected ^{26}Al/^{27}Al Ratio Uncertainty [a]	Background Corrected ^{26}Al/^{27}Al Ratio	Background Corrected ^{26}Al/^{27}Al Ratio Uncertainty	Measured ^{26}Al (atoms g^{-1})	^{26}Al Uncertainty (atoms g^{-1})	Measured ^{26}Al/^{10}Be	^{26}Al/^{10}Be Uncertainty	Cathode #
CF-02	Deglacial	20.46	0.0000	3.07E-14	2.91E-15	3.01E-14	2.91E-15	1.12E+05	1.08E+04	6.05	0.72	169432
LC-02	Deglacial	21.95	0.0000	7.50E-14	6.25E-15	7.45E-14	6.25E-15	1.27E+05	1.07E+04	5.44	0.57	169436
LC-04	Deglacial	19.74	0.6967	4.73E-14	4.80E-15	4.67E-14	4.80E-15	9.94E+04	1.02E+04	4.89	0.60	169438
LC-05	Deglacial	19.29	0.4114	4.11E-14	4.24E-15	4.05E-14	4.24E-15	1.60E+05	1.67E+04	5.72	0.71	169439
MC-01	Deglacial	19.60	0.2959	2.04E-14	2.39E-15	1.99E-14	2.39E-15	1.19E+05	1.43E+04	6.38	0.95	169441
MC-02	Deglacial	18.75	0.5855	5.66E-14	4.57E-15	5.61E-14	4.57E-15	1.17E+05	9.56E+03	6.27	0.73	169442
GB-03	Deglacial	9.38	0.0000	4.56E-15	1.83E-15	4.02E-15	1.83E-15	7.11E+04	3.23E+04	8.44	4.19	169444
GB-05	Deglacial	20.10	0.0000	3.01E-14	3.74E-15	2.95E-14	3.74E-15	1.76E+05	2.23E+04	8.02	1.25	169447
SS-01	Deglacial	19.70	0.4669	5.22E-14	4.66E-15	5.16E-14	4.66E-15	8.84E+04	7.98E+03	8.05	1.19	169450
SS-05	Deglacial	20.88	0.0000	1.09E-13	7.64E-15	1.09E-13	7.64E-15	3.99E+05	2.81E+04	7.15	0.61	169454
CF-01	Modern	18.52	0.0000	4.39E-14	4.56E-15	4.33E-14	4.56E-15	1.55E+05	1.63E+04	6.22	0.85	169431
CF-05	Modern	20.92	0.0000	1.04E-13	6.54E-15	1.03E-13	6.54E-15	3.67E+05	2.32E+04	7.02	0.53	169434
LC-01	Modern	20.41	0.3099	1.61E-13	8.24E-15	1.60E-13	8.24E-15	3.61E+05	1.85E+04	6.86	0.47	169435
LC-03	Modern	20.50	0.2586	1.74E-13	1.09E-14	1.73E-13	1.09E-14	3.80E+05	2.38E+04	6.82	0.52	169437
LC-06	Modern	19.44	0.7185	6.76E-14	5.83E-15	6.70E-14	5.83E-15	2.11E+05	1.84E+04	7.92	0.93	169440

GB-02	Modern	19.96	0.0000	5.02E-15	1.52E-15	4.48E-15	1.52E-15	1.02E+05	3.46E+04	7.24	2.56	169443
GB-04	Modern	17.34	0.0000	1.80E-15	1.20E-15	1.26E-15	1.20E-15	2.78E+04	2.65E+04	1.73	1.66	169445
MC-03	Modern	20.73	0.3872	6.21E-14	6.10E-15	6.16E-14	6.10E-15	1.20E+05	1.19E+04	6.06	0.79	169449
SS-02	Modern	20.37	0.6293	8.63E-14	6.19E-15	8.58E-14	6.19E-15	1.73E+05	1.25E+04	6.19	0.63	169451
SS-03	Modern	20.81	0.0000	5.02E-14	3.79E-15	4.97E-14	3.80E-15	1.72E+05	1.31E+04	6.55	0.67	169452
SS-04	Modern	22.15	0.0000	3.27E-14	4.20E-15	3.22E-14	4.21E-15	2.68E+05	3.51E+04	5.64	0.78	169453
GB-06	Bedrock	15.35	0.0000	1.62E-13	7.95E-15	1.62E-13	7.95E-15	5.91E+05	2.90E+04	8.05	0.58	169448

[a] Isotopic analysis conducted at PRIME Laboratory; ratios were normalized against standard KNSTD with an assumed ratio of 1.818×10^{-12} (Nishiizumi et al., 2004).

5.1 ^{10}Be and ^{26}Al Concentrations corrected for Holocene exposure

An average of ~19% (median ~15%) of ^{10}Be in deglacial samples was produced by subsurface exposure during the Holocene, with a range of 0.1-59.2% (Table 3). After correcting for Holocene nuclide production, the mean and median concentrations of ^{10}Be in this population of n=10 samples are $1.87 \pm 1.39 * 10^4$ atoms g^{-1} and $1.80 * 10^4$ atoms g^{-1}, respectively (Table 3). The percentage of ^{26}Al produced in deglacial samples after deposition ranged from 0.1-64.5%, with an average of ~22% (median = 14%). The modern samples have more ^{10}Be concentration variability, with an interquartile range (IQR) of $2.76 * 10^4$ atoms g^{-1} compared to the IQR of $9.02 * 10^3$ atoms g^{-1} for Holocene exposure-corrected deglacial samples.

We re-performed the Wilcoxon rank-sum tests using the Holocene exposure-corrected data. With ^{10}Be, there is a statistically significant difference between the mean concentrations of deglacial samples corrected for post-depositional production ($1.87 \pm 1.39 * 10^4$ atoms g^{-1}) and modern ($3.31 \pm 1.57 * 10^4$ atoms g^{-1}) samples (alpha = 0.05, p =0.020). For ^{26}Al, the mean concentration of deglacial ($1.20 \pm 1.04 * 10^5$ atoms g^{-1}) and modern ($2.12 \pm 1.18 * 10^5$ atoms g^{-1}) samples are also significantly different (alpha = 0.05, p =0.036).

Inherited concentrations in the bedrock sample (GB-06) were $2.47 * 10^4$ atoms g^{-1} ^{10}Be and $1.68 * 10^5$ atoms g^{-1} ^{26}Al when correcting for Holocene nuclide accumulation. This location is estimated to have deglaciated ~7.6 ka (Ullman et al., 2016). Taking into account the CRONUS calculated age of deglaciation (10,800±860 years), this is equivalent to inheritance from ~3.2 ka of surface exposure.

Table 3a. Assumptions for Holocene Corrected Concentrations

Sample Name	Deglaciation Age (yr) [a]	Sample Depth (cm) [b]	Depth Uncertainty (cm) [b]	^{10}Be Muon Production Rate (atoms g^{-1} y^{-1}) [c]	^{26}Al Muon Production Rate (atoms g^{-1} y^{-1}) [c]	^{10}Be Spallation Rate (atoms g^{-1} y^{-1}) [c]	^{26}Al Spallation Rate (atoms g^{-1} y^{-1}) [c]	Total ^{10}Be production rate at depth	Total ^{26}Al production rate at depth
CF-02	7500	800	-200, + 200	0.193	1.612	5.49	37.05	0.0745	0.6200
LC-02	7700	300	-100, +100	0.220	1.838	7.80	52.63	0.5074	3.6694
LC-04	7700	200	-50, + 100	0.212	1.774	7.11	47.98	1.0719	7.5030
LC-05	7700	200	-50, + 200	0.209	1.743	6.78	45.76	1.0276	7.1959
MC-01	8200	180	-30, + 70	0.217	1.811	7.49	50.50	1.3468	9.3599
MC-02	12800	2000	-200, + 200	0.181	1.513	4.54	30.61	0.0160	0.1334
GB-03	8000	700	-200, + 200	0.185	1.540	4.82	32.52	0.0826	0.6822
GB-05	8000	300	-100, + 100	0.211	1.759	6.96	46.94	0.4630	3.3559
SS-01	12800	550	-150, + 50	0.181	1.511	4.50	30.39	0.1084	0.8800
SS-05	12800	3000	-500, + 500	0.201	1.681	5.99	40.44	0.0053	0.0440

[a] Deglaciation ages estimated based on proximity to dated moraine systems in Ullman et al., 2016 and Dalton et al., 2020 isochrons (see methods).
[b] Sample depth estimated in the field. Depth uncertainty estimated from photos and field journal.
[c] Muonogenic and spallation production rates estimated from CRONUS online calculator using 07KNSTD AMS standard for Be and the KNSTD standard for Al.

Table 3b. Holocene Corrected Concentrations for Deglacial Samples

Sample Name	Inherited ^{10}Be (atoms g^{-1})	^{10}Be Uncertainty (atoms g^{-1}) [a]	Inherited ^{26}Al (atoms g^{-1})	^{26}Al Uncertainty (atoms g^{-1}) [a]	^{26}Al/^{10}Be at Time of Deposition	^{26}Al/^{10}Be Uncertainty [a]
CF-02	1.79E+04	- 1.32E+03, + 1.31E+03	1.07E+05	- 1.09E+04, + 1.08E+04	5.98	- 0.73, + 0.72
LC-02	1.95E+04	- 5.28E+03, + 2.38E+03	9.91E+04	- 3.61E+04, + 1.68E+04	5.08	- 0.83, + 0.59
LC-04	1.21E+04	- 4.96E+03, + 4.82E+03	4.17E+04	- 3.40E+04, + 3.31E+04	3.45	- 2.26, + 1.10
LC-05	2.00E+04	- 4.93E+03, + 6.36E+03	1.04E+05	- 3.51E+04, + 4.47E+04	5.22	- 0.85, + 0.81

MC-01	7.60E+03	- 3.89E+03, + 5.31E+03	4.23E+04	- 2.79E+04, + 3.71E+04	5.56	- 1.41, + 1.06
MC-02	1.85E+04	- 1.54E+03, + 1.54E+03	1.16E+05	- 9.57E+03, + 9.56E+03	6.24	- 0.73, + 0.73
GB-03	7.76E+03	- 1.72E+03, + 1.69E+03	6.56E+04	- 3.24E+04, + 3.23E+04	8.46	- 4.19, + 4.19
GB-05	1.82E+04	- 5.12E+03, + 2.66E+03	1.49E+05	- 3.90E+04, + 2.53E+04	8.18	- 1.34, + 1.26
SS-01	9.59E+03	- 1.61E+03, + 1.29E+03	7.72E+04	- 1.06E+04, + 8.06E+03	8.04	- 1.20, + 1.19
SS-05	5.58E+04	- 2.64E+03, + 2.63E+03	3.99E+05	- 2.81E+04, + 2.81E+04	7.15	- 0.61, + 0.61

[a] Uncertainty for both nuclides was calculated by propagating error from AMS data reduction with depth estimation error (see methods). Depth estimate uncertainty and changing production rates (based on depth) create asymmetrical uncertainty in both nuclide concentrations.

5.2 $^{26}Al/^{10}Be$ Ratios

Using concentrations corrected for ^{10}Be and ^{26}Al Holocene production in deglacial samples, the mean $^{26}Al/^{10}Be$ ratios for deglacial and modern samples are 6.34±1.61 and 6.20±1.61 respectively. The deglacial samples have much more ratio variability (IQR = 2.51) compared to modern samples (IQR = 0.82). There is a significant, positive linear trend for deglacial samples, with ratio values increasing with distance from the center of the Quebec-Labrador Ice Dome (alpha = 0.05, r =0.67, p = 0.034) (Figure 2). Modern samples, in contrast, exhibit no spatial trend in $^{26}Al/^{10}Be$ ratios.

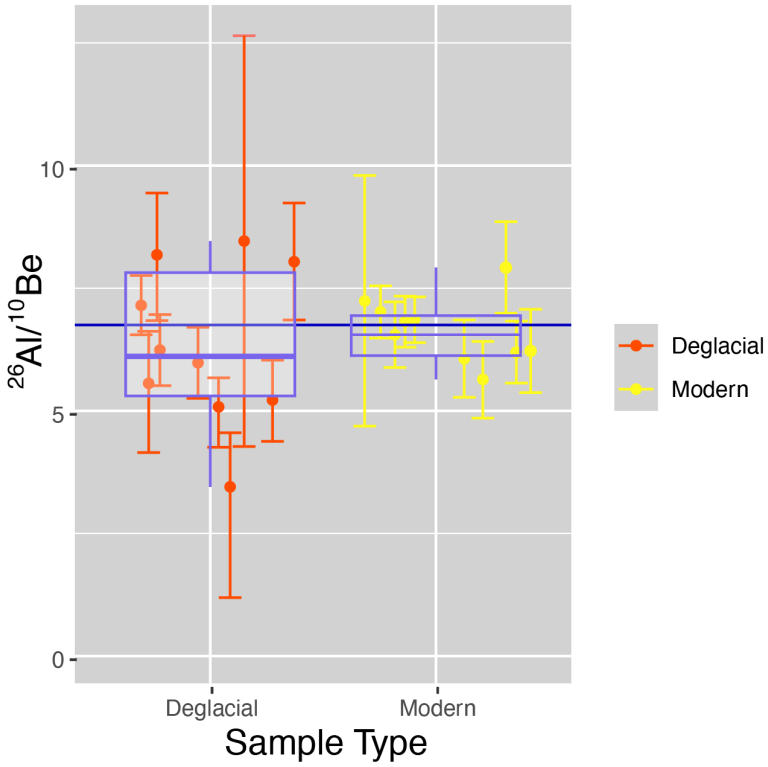

Figure 2. Nuclide Ratios for Deglacial Versus Modern Samples
Boxplots show the range and average of $^{26}Al/^{10}Be$ ratios for deglacial (Holocene corrected) and modern samples. The solid line indicates the nominal production ratio at high latitudes. Plotted points represent individual samples and are sorted by sample type. Error bars for modern samples represent combined AMS and extraction blank error. Error for deglacial samples is propagated from AMS, extraction blank, and depth estimate error (see methods). Sample LC-04 (modern) is excluded from the figure because the ^{26}Al measurement is not more than 2 SD above background.

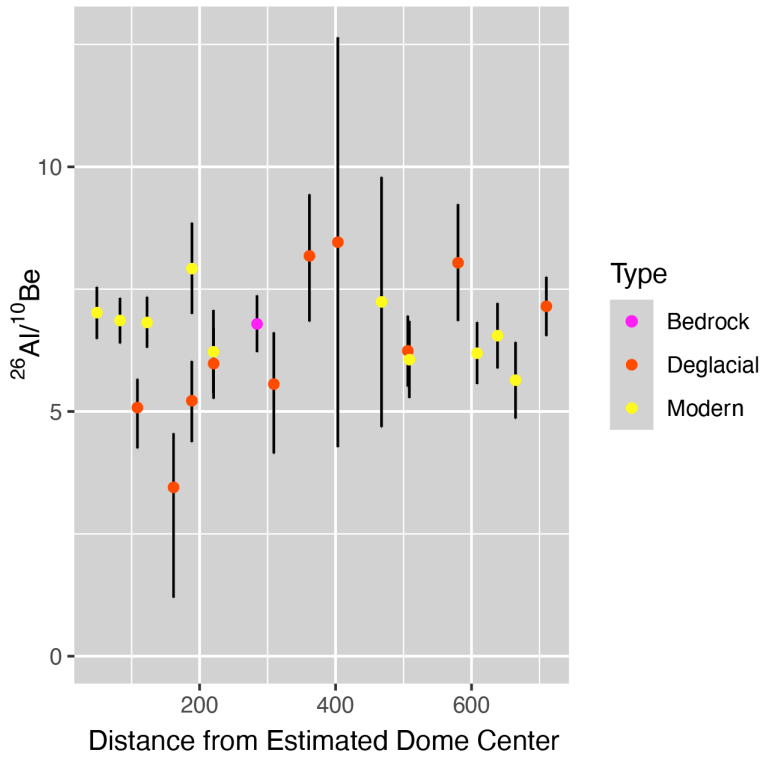

Figure 3. Spatial Variability in Nuclide Ratios
We used Labrador City as a proxy for the center of the Quebec-Labrador Ice Dome (Couette et al., 2023; Dalton et al., 2020). $^{26}Al/^{10}Be$ ratios for each sample are plotted and color coded by sample type. Ratios for the bedrock sample and deglacial samples are corrected for Holocene exposure. Error bars for modern samples represent combined AMS and extraction blank error. Error for bedrock and deglacial samples represent propagated AMS, extraction blank, and depth estimate error (see methods). Sample LC-04 (modern) is excluded from the figure because the ^{26}Al measurement is not more than 2 SD above background.

6. Discussion

Our data indicate that LIS erosion over Quebec and Labrador during the last glacial period was not sufficient or deep enough to remove cosmogenic nuclides accumulated during previous interglacials. Ratios of $^{26}Al/^{10}Be$ in deglacial sediments are near the production ratio of the two nuclides (7.3±0.3) at high latitudes (Corbett et al., 2017). This is a strong indication that Quebec-Labrador was ice free during interglacial period MIS5e at least. These findings of nuclide inheritance and thus minimal erosion are consistent with studies conducted in other regions of the LIS, as well as glacial and deglacial landscapes in Fennoscandia, Antarctica, and Greenland (e.g., Stroeven et al., 2002; Corbett et al., 2016; Briner & Swanson, 1998).

6.1 Nuclide Concentrations in Deglacial Sediments Indicate Limited Erosion by Laurentide Ice

After correcting for Holocene exposure, all deglacial sediment samples in our study (n=10) contain ^{26}Al and ^{10}Be inherited from exposure during prior interglacials. The center of the Quebec-Labrador

Ice Dome (approximately Labrador City) was covered by ice since at least ~70 ka and perhaps as early as ~115 ka (Dalton et al., 2022). Despite being buried for ~60-105 ka by the LIS during the last glacial period, nuclide concentrations have not been reset by erosion to zero. Subglacial process modeling over North America further supports a minimally erosive LIS in portions of Quebec and Labrador; specifically, modeling of the Quebec-Labrador region exhibits minimums for both basal sliding speed and total ice movement integrated over the last glacial cycle (Melanson et al., 2013) – both variables directly related to the efficacy of glacial erosion.

Ice sliding distance (the integrated basal velocity over the last glacial cycle in Mm) and velocity (m yr^{-1}) of the Quebec-Labrador Ice Dome are both modeled as near zero over the last glacial period in the central part of our study area. In other parts of our study area, ~1 Mm of sliding is modeled for the Goose Bay area, 1-2 Mm near the Manicouagan Reservoir, and 2.5 Mm near the St. Lawrence estuary (Melanson et al., 2013). Model results suggest sliding velocity was ~20 m yr^{-1} surrounding the Manicouagan Reservoir and ~30 m yr^{-1} on the banks of the St. Lawrence, compared to >750 m yr^{-1} for some parts of northeastern and midwestern North America (Melanson et al., 2013). Our data are consistent with modeling in that it supports this concept of a variably erosive LIS, containing multiple regions of slow ice movement and thus insignificant erosion where nuclides from prior periods of exposure are most likely to remain, such as the Quebec-Labrador Ice Dome.

Our results agree with ^{10}Be measurements made in bedrock and boulders by others as they attempted to date deglacial landforms in eastern Quebec. The one bedrock sample we analyzed (GB-06), which contained $2.47*10^4$ atoms g^{-1} of ^{10}Be inherited from a prior period of exposure (equivalent to about ~3 ka of surface exposure), was collected adjacent to samples CL3-10-01 (1.09 km from GB-06) and CL3-10-07 (0.65 km from GB-06) both along Ullman et al.'s (2016) CL3 transect (Figure 4). Ullman et al. excluded these boulder samples from their deglacial timing analysis because their estimated ages (~13.3 ka) were deemed too old. In total, 12 of 65 boulder samples from Ullman et al.'s (2023) analysis were regarded as outliers because of their unusually high concentration of ^{10}Be, all within the Quebec-Labrador region. Excluding outliers, measured ^{10}Be in samples results in ages ranging from 6.1±1.2 ka to 11.1±0.6 ka. Couette et al. (2023) similarly excluded 5 outliers in the Quebec-Labrador region because of high ^{10}Be concentrations, the result of inheritance from prior exposure. Calculated ^{10}Be exposure ages ranged from 7.9±0.3 ka to 13.3±0.5 ka (excluding outliers). These samples (moraine boulders) are also within the historical range of Quebec-Labrador ice, although further east towards the coast than our field area (Figure 5).

The abundance of glacially polished, rounded bedrock outcrops within our study site indicates that the ice dome was at one point warm-based and thus erosive. Our sample, GB-06, came from such a rounded bedrock outcrop (Figure 4). It is not possible to discern if this erosion occurred during the last glaciation or previous ones. It is highly unlikely that deglaciation and exposure to cosmic rays occurred during older interglacials such as MIS9 or MIS11 alone because $^{26}Al/^{10}Be$ ratios reflecting exposure that long ago would be lower (~4-5) than what we have observed (6.34±1.61, mean) due to more rapid decay of

^{26}Al. A Marshall-Clarke model (accounting for climate anomalies based on atmospheric circulation and spun up using paleoclimatic data from GRIP ice core from Greenland) indicates that during the LGM, a large portion of the south central LIS was likely cold-based (and thus non-erosive), as well as southwestern Hudson Bay and isolated pockets in Quebec-Labrador (Marshall et al., 2000). The average erosion depth for the whole LIS, integrated over the last glacial period, is estimated to be ~4 m and the modeled depth erosion within our study area ranges from 0 m (around the ice dome) to 1.8 m (Melanson et al., 2013). Such low amounts of erosion, in tandem with both shallow neutron and deep muon-induced nuclide production (Briner et al., 2016; Halstead et al., 2023) explains the nuclide inheritance we and others have measured.

Figure 4. GB-06
We sampled the peak of the outcrop near the pile of gear.

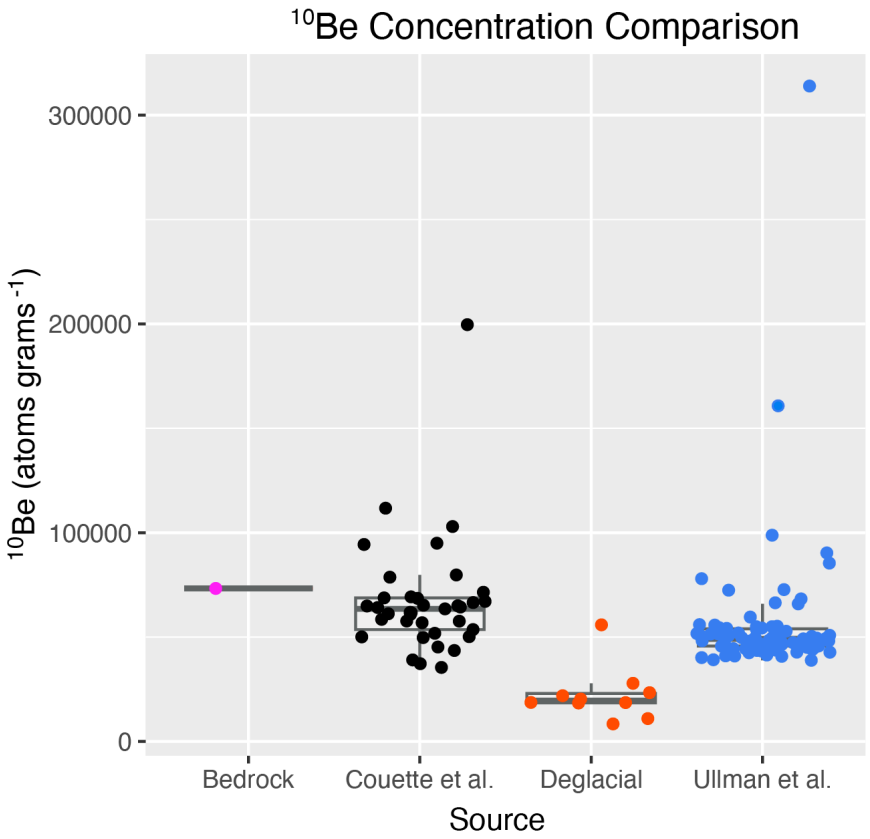

Figure 5. Comparison of ^{10}Be concentrations against Ullman et al. (2016) and Couette et al. (2023) Because no corrections for Holocene exposure were done in either study, measured ^{10}Be concentrations from our samples were used in this figure.

Outside of Quebec-Labrador, multiple studies provide evidence of cosmogenic nuclide inheritance in other portions of the LIS (e.g., Balco et al., 2005; Halstead et al., 2023; Davis et al., 1999; Colgan et al., 2002). A cobble sampled from Baffin Island had concentrations of ^{26}Al/^{10}Be that suggested ~3 ka years of inheritance (Davis et al., 1999). In the northeastern United States, Halstead et al. (2023) estimated that LIS terminal moraines had the equivalent of 2-6 ka of inherited ^{10}Be. In the midwestern United States, inherited ^{26}Al and ^{10}Be in glacial deposit outwash complicated efforts to date till deposits (Balco et al., 2005). In the Torngat Mountains of northern Labrador, measurements of ^{26}Al and ^{10}Be on bedrock sites and erratic boulders at mountain summits provide evidence of minimal erosion (<1.4 m Ma-1) where cold-based ice was predominant before deglaciation (Staiger et al., 2005). Three out of five bedrock outcrops sampled in south-central Wisconsin had concentrations of ^{26}Al and ^{10}Be eight times higher than predicted based on radiocarbon dating (Colgan et al., 2002). This corresponds to estimated glacial erosion rates of 0.01-0.25 mm yr^{-1}, providing further evidence that erosion must be many meters deep on the LIS deglacial landscape to reduce inherited nuclide concentrations to undetectable levels (Colgan et al., 2002).

Minimal erosion and inheritance of cosmogenic nuclides has been observed in areas once occupied by other ice sheets as well. In Antarctica, cobbles from the Ferrar glacier moraine adjacent to the

ice margin contain the equivalent ~50 ka ^{21}Ne (Staiger et al., 2006). On the historical periphery of the Scandinavian Ice Sheet, buried glacial erratic boulders had ~2 ka years of inherited muonogenic ^{10}Be (Briner et al., 2016). Towards the center of what was the Fennoscandian glaciation (northeastern Sweden), there is evidence that bedrock outcrops and boulder fields have been preserved through many glacial cycles since the late Cenozoic (Stroeven et al., 2002). Exposure ages for the tops of these outcrops ranged from 79 ka to 37 ka, even though the area deglaciated at ~11 ka (Stroeven et al., 2002). ^{26}Al/^{10}Be ratios suggest a minimum modeled history of 605 ka, which could include multiple interglacial exposure and subsequent burial events by the Fennoscandian Ice Sheet (Stroeven et al., 2002).

There is also evidence of minimal erosion near the margin of the Cordilleran Ice Sheet, with 8 out of 23 bedrock samples on Whitbey Island having ^{36}Cl/Cl ratios suggesting inheritance of nuclides produced from prior interglacials (Briner & Swanson, 1998). For this field area, erosion was estimated to be 0.09-0.35 mm yr^{-1}, making it possible that in the Puget Lowland, ice eroded only tens of meters of rock throughout the Quaternary (Briner & Swanson, 1998). In northwest Greenland, 8 of 28 sampled boulders had high concentrations of ^{10}Be and ^{26}Al along with ^{26}Al/^{10}Be ratios indicative of burial, providing evidence of minimal subglacial erosion over multiple interglacial and glacial periods where the ice was predominantly cold-based (Corbett et al., 2016). Despite the assumption that erosion and burial from ice sheets resets concentrations of cosmogenic nuclides to near-zero, there is ample evidence that ice sheets do not consistently remove nuclides created during prior periods of interglacial exposure.

6.2 Ratios Near Nominal Production Value Indicate the Ice Dome was not Persistent Throughout Pleistocene Interglacials

Finding lower than production ratios of ^{26}Al/^{10}Be in ice rafted debris (IRD) sourced from eastern Canada and deposited in the North Atlantic, LeBlanc et al. (2023) concluded that ice sheet remnants must have lingered across eastern Canada for the majority of interglacials. This IRD sourced from Heinrich layers is predominantly sourced from the LIS Hudson Strait ice stream during the last glaciation (LeBlanc et al., 2023). Data we present in this paper strongly suggests that the source of quartz analyzed by LeBlanc et al. was not within our field area because ^{26}Al/^{10}Be ratios from our deglacial samples are not depressed sufficiently to indicate burial over multiple Pleistocene interglacials. Ratios for our deglacial samples decrease the closer they are to the center of the ice dome, implying that ice persistence decreases radially outward from the center (Figure. 3). However, a Wilcoxon rank-sum test (alpha=0.05; p=0.00084) confirms that our deglacial Holocene-corrected ^{26}Al/^{10}Be ratios are significantly different from LeBlanc et al.'s (2023) IRD ratios. Furthermore, a one sample t-test confirms that our deglacial sample ^{26}Al/^{10}Be ratios are statistically inseparable from the production ratio of 7.3±0.3 (1σ) (alpha=0.05; p=0.l8). However, LeBlanc et al. 's ^{26}Al/^{10}Be IRD ratios are significantly different than 7.3±0.3 (1σ) using the same test (alpha=0.05; p<0.0000001). Therefore, it is unlikely that the IRD and our deglacial sediment are from the same population. Our data suggest that the Quebec-Labrador portion of the LIS went through multiple periods of

Plesitocene interglacial exposure (section 6.1), suggesting that LeBlanc et al.'s (2023) IRD may have been sourced from a more northern portion of the ice sheet that did not deglaciate during MIS5e.

However, $^{26}Al/^{10}Be$ ratios presented in LeBlanc et al. (2023) do agree with our finding that the eastern LIS was minimally erosive. Because IRD ratios are so low, it is likely that ^{26}Al and ^{10}Be were decaying in sediment for ~1 Ma before being transported to the deep sea. It is also possible that before becoming IRD, the sediment was stagnant at the bottom of Hudson Bay for hundreds of ka. This lag between deposition in Hudson Bay and transport by ice into the Atlantic Ocean entertains the possibility that the sediment had slightly higher ratios of $^{26}Al/^{10}Be$ (similar to the range of ratios in our deglacial data) when initially deposited by the ice stream, allowing $^{26}Al/^{10}Be$ to decay further until being transported as IRD. More extensive sampling of eastern Canada, including Quebec-Labrador, and further north near Hudson Bay and Baffin Island, would provide further evidence on how persistent eastern LIS was during Plesitocene interglacials.

Conclusions

Analysis of cosmogenic nuclides ^{26}Al and ^{10}Be in deglacial (n=10) and modern (n=11) sediments strongly suggests that the Quebec-Labrador Ice Dome was minimally erosive during the last glacial period, preserving nuclides created during prior interglacial exposures. Holocene exposure-corrected ratios of $^{26}Al/^{10}Be$ in deglacial samples are not statistically separable from the production ratio of those nuclides at high latitudes (7.3±0.3), implying that the ice dome deglaciated during MIS5e at least. Further sampling of this region, or northward near the Foxe-Baffin Dome, may provide more evidence of minimal erosion or where ice was persistent throughout Pleistocene interglacials—leading to the depressed $^{26}Al/^{10}Be$ ratios found in IRD from eastern LIS discharge.

Acknowledgements

We thank the 2022 field sampling team including Juliana Souza, Halley Mastro, and Cat Collins. We chose sample sites based on proximity to the Trans-Labrador Highway and Route 389 following suggestions from Dr. Pierre-Olivier Couette. Funding for this research was provided by NSF-EAR-2116209,-1735676 and -1735676 to Bierman and Corbett.

References

Abe-Ouchi, A., Saito, F., Kawamura, K., Raymo, M. E., Okuno, J., Takahashi, K., & Blatter, H. (2013). Insolation-driven 100,000-year glacial cycles and hysteresis of ice-sheet volume. *Nature*, *500*(7461), 190–193. https://doi.org/10.1038/nature12374

Amani, M., Mahdavi, S., Afshar, M., Brisco, B., Huang, W., Mirzadeh, S. M. J., White, L., Banks, S. N., Montgomery, J., & Hopkinson, C. (2019). Canadian Wetland Inventory using Google Earth Engine: The First Map and Preliminary Results. *Remote Sensing*, *11*(7), 842. https://doi.org/10.3390/rs11070842

Andrews, J. T., & Tyler, K. L. (2011). The observed postglacial recovery of Québec and Nouveau-Québec Since 12,000 BP. *Géographie Physique Et Quaternaire*, *31*(3–4), 389–400. https://doi.org/10.7202/1000286ar

Balco, G., Stone, J. O. H., & Jennings, C. (2005). Dating Plio-Pleistocene glacial sediments using the cosmic-ray-produced radionuclides ^{10}Be and ^{26}Al. *American Journal of Science*, *305*(1), 1–41. https://doi.org/10.2475/ajs.305.1.1

Batchelor, C. L., Margold, M., Krapp, K., Murton, D. K., Dalton, A. S., Gibbard, P. L., Stokes, C. R., Murton, J. B., & Manica, A. (2019). The configuration of Northern Hemisphere ice sheets through the Quaternary. *Nature Communications, 10.* https://doi.org/10.1038/s41467-019-11601-2

Beck, H. E., Zimmermann, N. E., McVicar, T. R., Vergopolan, N., Berg, A., & Wood, E. F. (2018). Present and future Köppen-Geiger climate classification maps at 1-km resolution. *Scientific Data*, *5*(1). https://doi.org/10.1038/sdata.2018.214

Bierman, P. (1994). Using in situ produced cosmogenic isotopes to estimate rates of landscape evolution: A review from the geomorphic perspective. *Journal of Geophysical Research, 99*(10), 13.885-13.896

Bierman, P. R., Marsella, K. A., Patterson, C. J., Davis, P. T., & Caffee, M. W. (1999). Mid-Pleistocene cosmogenic minimum-age limits for pre-Wisconsinan glacial surfaces in southwestern Minnesota and southern Baffin Island: a multiple nuclide approach. *Geomorphology*, *27*(1–2), 25–39. https://doi.org/10.1016/s0169-555x(98)00088-9

Bierman, P. R., Shakun, J. D., Corbett, L. B., Zimmerman, S., & Rood, D. H. (2016). A persistent and dynamic East Greenland Ice Sheet over the past 7.5 million years. *Nature*, *540*(7632), 256–260. https://doi.org/10.1038/nature20147

Bintanja, R., & Van De Wal, R. S. W. (2008). North American ice-sheet dynamics and the onset of 100,000-year glacial cycles. *Nature*, *454*(7206), 869–872. https://doi.org/10.1038/nature07158

Braucher, R., Brown, E. T., Bourlès, D., & Colin, F. (2003). In situ produced 10Be measurements at great depths: implications for production rates by fast muons. *Earth and Planetary Science Letters*, *211*(3–4), 251–258. https://doi.org/10.1016/s0012-821x(03)00205-x

Braucher, R., Merchel, S., Borgomano, J., & Bourlès, D. (2011). Production of cosmogenic radionuclides at great depth: A multi element approach. *Earth and Planetary Science Letters*, *309*(1–2), 1–9. https://doi.org/10.1016/j.epsl.2011.06.036

Briner, J. P., Goehring, B. M., Mangerud, J., & Svendsen, J. I. (2016). The deep accumulation of 10Be at Utsira, southwestern Norway: Implications for cosmogenic nuclide exposure dating in peripheral ice sheet landscapes. *Geophysical Research Letters*, *43*(17), 9121–9129. https://doi.org/10.1002/2016gl070100

Briner, J. P., & Swanson, T. W. (1998). Using inherited cosmogenic 36Cl to constrain glacial erosion rates of the Cordilleran ice sheet. *Geology | GeoScienceWorld*. https://doi.org/10.1130/0091-7613(1998)026

Colgan, P. M., Bierman, P. R., Mickelson, D. M., & Caffee, M. (2002). Variation in glacial erosion near the southern margin of the Laurentide Ice Sheet, south-central Wisconsin, USA: Implications for cosmogenic dating of glacial terrains. *GSA Bulletin | GeoScienceWorld*. https://doi.org/10.1130/0016-7606(2002)114

Corbett, L. B., Bierman, P. R. and Davis, P.T. (2016) Glacial history and landscape evolution of southern Cumberland Peninsula, Baffin Island, Canada, constrained by cosmogenic ^{10}Be and ^{26}Al. Geological Society of America Bulletin. v. 128(7-8), p. 1173-1192. doi.org/10.1130/B31402.1

Corbett, L. B., Bierman, P. R., Neumann, T., Graly, J. A., Shakun, J. D., Goehring, B. M., Hidy, A. J., &

Caffee, M. W. (2021). Measuring multiple cosmogenic nuclides in glacial cobbles sheds light on Greenland Ice Sheet processes. *Earth and Planetary Science Letters*, *554*, 116673. https://doi.org/10.1016/j.epsl.2020.116673

Corbett, L. B., Bierman, P. R., & Rood, D. H. (2016a). An approach for optimizing in situ cosmogenic 10Be sample preparation. *Quaternary Geochronology*, *33*, 24–34. https://doi.org/10.1016/j.quageo.2016.02.001

Corbett, L. B., Bierman, P. R. and Rood, D. H. (2016b) Constraining multi-stage exposure-burial scenarios for boulders preserved beneath cold-based glacial ice in Thule, Northwest Greenland. *Earth and Planetary Science Letters*, *440*, 147–157. doi.org/10.1016/j.epsl.2016.02.004

Corbett, L. B., Bierman, P. R., Rood, D. H., Caffee, M. W., Lifton, N. A. and Woodruff, T. E. (2017), Cosmogenic $^{26}Al/^{10}Be$ surface production ratio in Greenland. *Geophysical Research Letters*, *44*(3), 1350-1359. doi.org/10.1002/2016GL071276

Couette, P., Ghienne, J., Lajeunesse, P., & Woerd, J. (2023). Climatic control on the retreat of the Laurentide Ice Sheet margin in easternmost Québec–Labrador (Canada) revealed by cosmogenic nuclide exposure dating. *Journal of Quaternary Science, 38*(7), 1044-1061. https://doi.org/10.1002/jqs.3525

Dalton, A., Finkelstein, S. A., Forman, S. L., Barnett, P. J., Pico, T., & Mitrovica, J. X. (2019). Was the Laurentide Ice Sheet significantly reduced during Marine Isotope Stage 3? *Geology*, *47*(2), 111–114. https://doi.org/10.1130/g45335.1

Dalton, A., Margold, M., Stokes, C., Tarasov, L., Dyke, A. S., Adams, R. S., Allard, S., Atends, H. E., Atkinson, N., Attig, J. W., Barnett, P., Barnett, R., Batterson, M., Bernatchez, P., Borns, H. W., Breckenridge, A., Briner, J. P., Brouard, E., Campbell, J. E., Carlson, A. E.,..., Wright, H. E. (2020). An Updated Radiocarbon-Based Ice Margin Chronology for the Last Deglaciation of the North American Ice Sheet Complex. *Quaternary Science Reviews, 234*(15), 0277-3791. https://doi.org/10.1016/j.quascirev.2020.106223

Davis, P. T., Bierman, P. R., Marsella, K. A., Caffee, M. W., & Southon, J. (1999). Cosmogenic analysis of glacial terrains in the eastern Canadian Arctic: a test for inherited nuclides and the effectiveness of glacial erosion. *Annals of Glaciology*, *28*, 181–188. https://doi.org/10.3189/172756499781821805

Dunai, T. J., & Lifton, N. A. (2014). The nuts and bolts of cosmogenic nuclide production. *Elements*, *10*(5), 347–350. https://doi.org/10.2113/gselements.10.5.347

Dyke, A. S. (2004). An outline of North American deglaciation with emphasis on central and northern Canada. In *Developments in quaternary science* (pp. 373–424). https://doi.org/10.1016/s1571-0866(04)80209-4

Goehring, B. M., Kelly, M. A., Schaefer, J. M., Finkel, R. C., & Lowell, T. V. (2010). Dating of raised marine and lacustrine deposits in east Greenland using beryllium‐10 depth profiles and implications for estimates of subglacial erosion. *JQS. Journal of Quaternary Science/Journal of Quaternary Science*, *25*(6), 865–874. https://doi.org/10.1002/jqs.1380

Gosse, J. C., & Phillips, F. M. (2001). Terrestrial in situ cosmogenic nuclides: theory and application. *Quaternary Science Reviews*, *20*(14), 1475–1560. https://doi.org/10.1016/s0277-3791(00)00171-2

Gregoire, L., Ivanović, R., Maycock, A. C., Valdes, P. J., & Stevenson, S. (2018). Holocene lowering of the Laurentide ice sheet affects North Atlantic gyre circulation and climate. *Climate Dynamics*, *51*(9–10), 3797–3813. https://doi.org/10.1007/s00382-018-4111-9

Halsted, C. T., Bierman, P. R., Shakun, J. D., Davis, P. T., Corbett, L. B., Drebber, J. S., & Ridge, J. C. (2023). A critical re-analysis of constraints on the timing and rate of Laurentide Ice Sheet recession in the northeastern United States. *JQS. Journal of Quaternary Science/Journal of Quaternary Science*, *39*(1), 54–69. https://doi.org/10.1002/jqs.3563

Harbor, J. M., Stroeven, A. P., Fabel, D., Clarhäll, A., Klemån, J., Li, Y., Elmore, D., & Fink, D. (2006). Cosmogenic nuclide evidence for minimal erosion across two subglacial sliding boundaries of the late glacial Fennoscandian ice sheet. *Geomorphology*, *75*(1–2), 90–99. https://doi.org/10.1016/j.geomorph.2004.09.036

Hynes, A., & Rivers, T. (2010). Protracted continental collision — evidence from the Grenville Orogen.

This article is one of a series of papers published in this Special Issue on the theme Lithoprobe — parameters, processes, and the evolution of a continent. *Canadian Journal of Earth Sciences*, *47*(5), 591–620. https://doi.org/10.1139/e10-003

Klein, J., Giegengack, R., Middleton, R., & Weeks, R. (1986). Revealing histories of exposure using insitu produced AL-26 and BE-10 in Libyan desert glass. *Radiocarbon*, *28*(547-555).

Kleman, J., Borgstrom, I., & Hattestrand, C. (1994). Evidence for a relict glacial landscape in Quebec-Labrador. Palaeogeography, Palaeoclimatology, Palaeoecology, 111(1994), 217-228.

Klemån, J., Jansson, K. N., De Angelis, H., Stroeven, A. P., Hättestrand, C., Alm, G., & Glasser, N. F. (2010). North American Ice Sheet build-up during the last glacial cycle, 115–21 kyr. *Quaternary Science Reviews*, *29*(17–18), 2036–2051. https://doi.org/10.1016/j.quascirev.2010.04.021

LeBlanc, D. E., Shakun, J. D., Corbett, L. B., Bierman, P. R., Caffe, M. W., & Hidy, A. J. (2023). Laurentide Ice Sheet Persistence During Pleistocene Interglacials. *Geology, 51*(5), 496-499. https://doi.org/10.1130/G50820.1

Larue, F., Royer, A., De Sève, D., Langlois, A., Roy, A., & Brucker, L. (2017). Validation of GlobSnow-2 snow water equivalent over Eastern Canada. *Remote Sensing of Environment*, *194*, 264–277. https://doi.org/10.1016/j.rse.2017.03.027

Margold, M., Stokes, C. R., & Clark, C. D. (2018). Reconciling records of ice streaming and ice margin retreat to produce a palaeogeographic reconstruction of the deglaciation of the Laurentide Ice Sheet. *Quaternary Science Reviews*, *189*, 1–30. https://doi.org/10.1016/j.quascirev.2018.03.013

Marsella, K. A., Bierman, P. R., Davis, P. T. and Caffee, M. W. (2000) Cosmogenic ^{10}Be and ^{26}Al ages for the last glacial maximum, eastern Baffin Island, Arctic Canada. *Geological Society of America Bulletin*. v. 112(8), p. 1296-1312. doi.org/10.1130/0016-7606(2000)112<1296:CBAAAF>2.0.CO;2

Marshall, S. J., Tarasov, L., Clarke, G. K. C., & Peltier, W. R. (2000). Glaciological reconstruction of the Laurentide Ice Sheet: physical processes and modelling challenges. *Canadian Journal of Earth Sciences*, *37*(5), 769–793. https://doi.org/10.1139/e99-113

Melanson, A., Bell, T., & Tarasov, L. (2013). Numerical modelling of subglacial erosion and sediment transport and its application to the North American ice sheets over the Last Glacial cycle. *Quaternary Science Reviews*, *68*, 154–174. https://doi.org/10.1016/j.quascirev.2013.02.017

Miller, G. H., & Andrews, J. T. (2019). Hudson Bay was not deglaciated during MIS-3. *Quaternary Science Reviews*, *225*, 105944. https://doi.org/10.1016/j.quascirev.2019.105944

Munroe, J. S., Perzan, Z., & Amidon, W. H. (2016). Cave sediments constrain the latest Pleistocene advance of the Laurentide Ice Sheet in the Champlain Valley, Vermont, USA. *JQS. Journal of Quaternary Science/Journal of Quaternary Science*, *31*(8), 893–904. https://doi.org/10.1002/jqs.2913

Nelson, A. H., Bierman, P. R., Shakun, J. D., & Hood, D. H. (2014). Using in situ cosmogenic 10Be to identify the source of sediment leaving Greenland. *Earth Surface Processes and Landforms, 39*, 1087-1100. 10.1002/esp.3565

Nishiizumi, K. (2004). Preparation of 26Al AMS standards. *Nuclear Instruments and Methods in Physics Research. Section B, Beam Interactions With Materials and Atoms/Nuclear Instruments & Methods in Physics Research. Section B, Beam Interactions With Materials and Atoms*, *223–224*, 388–392. https://doi.org/10.1016/j.nimb.2004.04.075

Nishiizumi, K., Kohl, C. P., Arnold, J. R., Klein, J., Fink, D., & Middleton, R. (1991). Cosmic ray produced 10Be and 26Al in Antarctic rocks: exposure and erosion history. *Earth and Planetary Science Letters*, *104*(2–4), 440–454. https://doi.org/10.1016/0012-821x(91)90221-3

Nishiizumi, K., Imamura, M., Caffee, M. W., Southon, J., Finkel, R. C., & McAninch, J. (2007). Absolute calibration of ^{10}Be AMS standards. *Nuclear Instruments and Methods in Physics Research. Section B, Beam Interactions With Materials and Atoms/Nuclear Instruments & Methods in Physics Research. Section B, Beam Interactions With Materials and Atoms*, *258*(2), 403–413. https://doi.org/10.1016/j.nimb.2007.01.297

Nishiizumi, K., Winterer, E. L., Kohl, C. P., Klein, J., Middleton, R., Lal, D., & Arnold, J. R. (1989). Cosmic ray production rates of 10Be and 26Al in quartz from glacially polished rocks. *Journal of Geophysical Research*, *94*(B12), 17907–17915. https://doi.org/10.1029/jb094ib12p17907

Payette, S., Morneau, C., Sirois, L., & Desponts, M. (1989). Recent fire history of the Northern Quebec Biomes. *Ecology*, *70*(3), 656–673. https://doi.org/10.2307/1940217

Pico, T., Birch, L., Weisenberg, J., & Mitrovica, J. (2018). Refining the Laurentide Ice Sheet at Marine Isotope Stage 3: A data-based approach combining glacial isostatic simulations with a dynamic ice model. *Quaternary Science Reviews*, *195*, 171–179. https://doi.org/10.1016/j.quascirev.2018.07.023

Rasmussen, S. O., Andersen, K. H., Svensson, A., Steffensen, J. P., Vinther, B. M., Clausen, H., Siggaard-Andersen, M., Johnsen, S. J., Larsen, L. H., Dahl-Jensen, D., Bigler, M., Röthlisberger, R., Fischer, H., Goto-Azuma, K., Hansson, M., & Ruth, U. (2006). A new Greenland ice core chronology for the last glacial termination. *Journal of Geophysical Research*, *111*(D6). https://doi.org/10.1029/2005jd006079

Rivers of Canada - Churchill River : Can Geo Education. (n.d.). https://web.archive.org/web/20200201124628/http://www.cangeoeducation.ca/resources/rivers_of_canada/churchill_river/default.asp

Roy, M., Hemming, S. R., & Parent, M. (2009). Sediment sources of northern Québec and Labrador glacial deposits and the northeastern sector of the Laurentide Ice Sheet during ice-rafting events of the last glacial cycle. *Quaternary Science Reviews*, *28*(27–28), 3236–3245. https://doi.org/10.1016/j.quascirev.2009.08.008

Spray, J. G., Kelley, S. P., & Rowley, D. B. (1998). Evidence for a late Triassic multiple impact event on Earth. *Nature*, *392*(6672), 171–173. https://doi.org/10.1038/32397

Staiger, J. K. W., Gosse, J. C., Johnson, J. V., Fastook, J. L., Gray, J., Stöckli, D. F., Stockli, L. D., & Finkel, R. C. (2005). Quaternary relief generation by polythermal glacier ice. *Earth Surface Processes and Landforms*, *30*(9), 1145–1159. https://doi.org/10.1002/esp.1267

Staiger, J. W., Marchant, D. R., Schaefer, J. M., Oberholzer, P., Johnson, J. V., Lewis, A. R., & Swanger, K. M. (2006). Plio-Pleistocene history of Ferrar Glacier, Antarctica: Implications for climate and ice sheet stability. *Earth and Planetary Science Letters*, *243*(3–4), 489–503. https://doi.org/10.1016/j.epsl.2006.01.037

Stokes, C. R., Tarasov, L., & Dyke, A. S. (2012). Dynamics of the North American Ice Sheet Complex during its inception and build-up to the Last Glacial Maximum. *Quaternary Science Reviews*, *50*, 86–104. https://doi.org/10.1016/j.quascirev.2012.07.009

Stroeven, A. P., Fabel, D., Hättestrand, C., & Harbor, J. M. (2002). A relict landscape in the centre of Fennoscandian glaciation: cosmogenic radionuclide evidence of tors preserved through multiple glacial cycles. *Geomorphology*, *44*(1–2), 145–154. https://doi.org/10.1016/s0169-555x(01)00150-7

Süfke, F., Gutjahr, M., Keigwin, L. D., Reilly, B. T., Giosan, L., & Lippold, J. (2022). Arctic drainage of Laurentide Ice Sheet meltwater throughout the past 14,700 years. *Communications Earth & Environment*, *3*(1). https://doi.org/10.1038/s43247-022-00428-3

Tarasov, L., Dyke, A. S., Neal, R. M., & Peltier, W. R. (2012). A data-calibrated distribution of deglacial chronologies for the North American ice complex from glaciological modeling. *Earth and Planetary Science Letters*, *315–316*, 30–40. https://doi.org/10.1016/j.epsl.2011.09.010

Ullman, D. (2023). The retreat chronology of the Laurentide Ice Sheet during the last 10,000 years and implications for deglacial sea-level rise. *Vignettes: Key Concepts in Geomorphology.* https://serc.carleton.edu/59463.

Ullman, D., Carlson, A. E., Hostetler, S. W., Clark, P. U., Cuzzone, J., Milne, G. A., Windsor, K., & Caffe, M. (2016). Final Laurentide ice-sheet deglaciation and Holocene climate-sea level change. *Quaternary Science Reviews, 152*(15), 49.59. https://doi.org/10.1016/j.quascirev.2016.09.014

Chapter 3. Reflections and Next Steps

Reflections on Study Design and Execution

In July 2022, the field team acquired only two bedrock outcrop samples in addition to the sediment samples. Of these two, only GB-06 had a sufficient amount of quartz to extract ^{10}Be and ^{26}Al. Because GB-06 had higher concentrations of both nuclides in comparison to the deglacial sediment samples, I am curious if more extensive sampling of bedrock outcrops in the same study area will yield similar results of high ^{10}Be and ^{26}Al inheritance. It is also possible that in a larger pool of samples, GB-06 would act as an outlier, similar to Ullman et al. (2016) and Couette et al's. (2023) data where multiple samples with high nuclide inheritance were excluded from exposure dating analysis (see Chapter 2: Figure 5 and section 6.1). Ideally, collecting n~10 of bedrock outcrop samples would have been best to allow for more robust statistical comparisons between the three sample types (bedrock, deglacial sediment, and modern river sediment) with approximately equal sizes.

We originally planned to have two field seasons in the Quebec-Labrador Ice Dome region: one sampling along the Trans-Labrador highway (completed in July 2022) and another sampling along the Trans-Taiga road. However, due to the 2023 Canadian wildfires, the second field excursion was not feasible. Observing ^{26}Al and ^{10}Be inheritance in bedrock and deglacial sediment samples along the Trans-Taiga road would further support our conclusion of a minimally erosive Quebec-Labrador Ice Dome during the last glacial cycle. This would give us more confidence in extrapolating our findings outside of our 2022 study area to a greater extent of the ice dome. If ^{26}Al/^{10}Be ratios from deglacial sediment samples along the Trans-Taiga transect were similar to what we have already measured, there would be more evidence in favor of ice dome deglaciation during (at least) MIS5e.

I also wish that I had been able to involve communities local to our field area, especially Indigenous communities, in research phases such as fieldwork and manuscript writing. Working with Arctic Indigenous communities such as the Inuit would have added another dimension to the research, making the results more accessible to the populations who have inhabited eastern Subarctic Canada for generations. I wanted to make these connections before our 2023 field season. However, the wildfires in the region prevented any further work there. Realistically, it takes six months to one year to build an equitable working relationship with Indigenous communities before starting research collaboration. This becomes difficult with the compressed timeline of a two-year master's degree. However, I have realized that this is something I am interested in pursuing during my future doctorate work.

Potential Work Moving Forward

Up until the first week of June, I will continue working on the journal manuscript in chapter 2, addressing committee commentary from my defense as well as preparing to submit it for review to *Geochronology.* Aside from addressing reviewer commentary, I hope to remain involved in the eventual analysis of ^{26}Al and ^{10}Be data extracted from Alaskan sediment samples where I was part of the sampling

team. I anticipate easily being able to apply data analysis techniques learned in the past two years to this project, part of a colleague's doctoral work on paleo-ice sheet erosion.

There was a possibility of me being a part of more LIS fieldwork. Our principal investigators applied for additional funding to sample around the Foxe-Baffin Ice Dome (further north of Quebec-Labrador). We are curious if $^{26}Al/^{10}Be$ ratios measured in deglacial sediment near Foxe-Baffin will be more depressed (~4.5) than what we measured in deglacial sediments from Quebec-Labrador. If funding is eventually approved for more time in the field, I am eager to be a part of the sampling team.

References

Couette, P., Ghienne, J., Lajeunesse, P., & Woerd, J. (2023). Climatic control on the retreat of the Laurentide Ice Sheet margin in easternmost Québec–Labrador (Canada) revealed by cosmogenic nuclide exposure dating. *Journal of Quaternary Science, 38*(7), 1044-1061. https://doi.org/10.1002/jqs.3525

Ullman, D., Carlson, A. E., Hostetler, S. W., Clark, P. U., Cuzzone, J., Milne, G. A., Windsor, K., & Caffe, M. (2016). Final Laurentide ice-sheet deglaciation and Holocene climate-sea level change. *Quaternary Science Reviews, 152*(15), 49.59. https://doi.org/10.1016/j.quascirev.2016.09.014

Comprehensive Bibliography

Abe-Ouchi, A., Saito, F., Kawamura, K., Raymo, M. E., Okuno, J., Takahashi, K., & Blatter, H. (2013). Insolation-driven 100,000-year glacial cycles and hysteresis of ice-sheet volume. *Nature*, *500*(7461), 190–193. https://doi.org/10.1038/nature12374

Amani, M., Mahdavi, S., Afshar, M., Brisco, B., Huang, W., Mirzadeh, S. M. J., White, L., Banks, S. N., Montgomery, J., & Hopkinson, C. (2019). Canadian Wetland Inventory using Google Earth Engine: The First Map and Preliminary Results. *Remote Sensing*, *11*(7), 842. https://doi.org/10.3390/rs11070842

Andrews, J. T., & Tyler, K. L. (2011). The observed postglacial recovery of Québec and Nouveau-Québec Since 12,000 BP. *Géographie Physique Et Quaternaire*, *31*(3–4), 389–400. https://doi.org/10.7202/1000286ar

Balco, G., Stone, J. O. H., & Jennings, C. (2005). Dating Plio-Pleistocene glacial sediments using the cosmic-ray-produced radionuclides ^{10}Be and ^{26}Al. *American Journal of Science*, *305*(1), 1–41. https://doi.org/10.2475/ajs.305.1.1

Batchelor, C. L., Margold, M., Krapp, K., Murton, D. K., Dalton, A. S., Gibbard, P. L., Stokes, C. R., Murton, J. B., & Manica, A. (2019). The configuration of Northern Hemisphere ice sheets through the Quaternary. *Nature Communications, 10.* https://doi.org/10.1038/s41467-019-11601-2

Beck, H. E., Zimmermann, N. E., McVicar, T. R., Vergopolan, N., Berg, A., & Wood, E. F. (2018). Present and future Köppen-Geiger climate classification maps at 1-km resolution. *Scientific Data*, *5*(1). https://doi.org/10.1038/sdata.2018.214

Bierman, P. (1994). Using in situ produced cosmogenic isotopes to estimate rates of landscape evolution: A review from the geomorphic perspective. *Journal of Geophysical Research, 99*(10), 13.885-13.896

Bierman, P. R., Marsella, K. A., Patterson, C. J., Davis, P. T., & Caffee, M. W. (1999). Mid-Pleistocene cosmogenic minimum-age limits for pre-Wisconsinan glacial surfaces in southwestern Minnesota and southern Baffin Island: a multiple nuclide approach. *Geomorphology*, *27*(1–2), 25–39. https://doi.org/10.1016/s0169-555x(98)00088-9

Bierman, P. R., Shakun, J. D., Corbett, L. B., Zimmerman, S., & Rood, D. H. (2016). A persistent and dynamic East Greenland Ice Sheet over the past 7.5 million years. *Nature*, *540*(7632), 256–260. https://doi.org/10.1038/nature20147

Bintanja, R., & Van De Wal, R. S. W. (2008). North American ice-sheet dynamics and the onset of 100,000-year glacial cycles. *Nature*, *454*(7206), 869–872. https://doi.org/10.1038/nature07158

Braucher, R., Brown, E. T., Bourlès, D., & Colin, F. (2003). In situ produced 10Be measurements at great depths: implications for production rates by fast muons. *Earth and Planetary Science Letters*, *211*(3–4), 251–258. https://doi.org/10.1016/s0012-821x(03)00205-x

Braucher, R., Merchel, S., Borgomano, J., & Bourlès, D. (2011). Production of cosmogenic radionuclides at great depth: A multi element approach. *Earth and Planetary Science Letters*, *309*(1–2), 1–9. https://doi.org/10.1016/j.epsl.2011.06.036

Briner, J. P., Goehring, B. M., Mangerud, J., & Svendsen, J. I. (2016). The deep accumulation of 10Be at Utsira, southwestern Norway: Implications for cosmogenic nuclide exposure dating in peripheral ice sheet landscapes. *Geophysical Research Letters*, *43*(17), 9121–9129. https://doi.org/10.1002/2016gl070100

Briner, J. P., & Swanson, T. W. (1998). Using inherited cosmogenic 36Cl to constrain glacial erosion rates of the Cordilleran ice sheet. *Geology | GeoScienceWorld*. https://doi.org/10.1130/0091-7613(1998)026

Colgan, P. M., Bierman, P. R., Mickelson, D. M., & Caffee, M. (2002). Variation in glacial erosion near the southern margin of the Laurentide Ice Sheet, south-central Wisconsin, USA: Implications for cosmogenic dating of glacial terrains. *GSA Bulletin | GeoScienceWorld*. https://doi.org/10.1130/0016-7606(2002)114

Corbett, L. B., Bierman, P. R. and Davis, P.T. (2016) Glacial history and landscape evolution of southern

Cumberland Peninsula, Baffin Island, Canada, constrained by cosmogenic ^{10}Be and ^{26}Al. Geological Society of America Bulletin. v. 128(7-8), p. 1173-1192. doi.org/10.1130/B31402.1

Corbett, L. B., Bierman, P. R., Neumann, T., Graly, J. A., Shakun, J. D., Goehring, B. M., Hidy, A. J., & Caffee, M. W. (2021). Measuring multiple cosmogenic nuclides in glacial cobbles sheds light on Greenland Ice Sheet processes. *Earth and Planetary Science Letters*, *554*, 116673. https://doi.org/10.1016/j.epsl.2020.116673

Corbett, L. B., Bierman, P. R., & Rood, D. H. (2016a). An approach for optimizing in situ cosmogenic 10Be sample preparation. *Quaternary Geochronology*, *33*, 24–34. https://doi.org/10.1016/j.quageo.2016.02.001

Corbett, L. B., Bierman, P. R. and Rood, D. H. (2016b) Constraining multi-stage exposure-burial scenarios for boulders preserved beneath cold-based glacial ice in Thule, Northwest Greenland. *Earth and Planetary Science Letters*, *440*, 147–157. doi.org/10.1016/j.epsl.2016.02.004

Corbett, L. B., Bierman, P. R., Rood, D. H., Caffee, M. W., Lifton, N. A. and Woodruff, T. E. (2017), Cosmogenic ^{26}Al/^{10}Be surface production ratio in Greenland. *Geophysical Research Letters*, *44*(3), 1350-1359. doi.org/10.1002/2016GL071276

Couette, P., Ghienne, J., Lajeunesse, P., & Woerd, J. (2023). Climatic control on the retreat of the Laurentide Ice Sheet margin in easternmost Québec–Labrador (Canada) revealed by cosmogenic nuclide exposure dating. *Journal of Quaternary Science, 38*(7), 1044-1061. https://doi.org/10.1002/jqs.3525

Dalton, A., Finkelstein, S. A., Forman, S. L., Barnett, P. J., Pico, T., & Mitrovica, J. X. (2019). Was the Laurentide Ice Sheet significantly reduced during Marine Isotope Stage 3? *Geology*, *47*(2), 111–114. https://doi.org/10.1130/g45335.1

Dalton, A., Margold, M., Stokes, C., Tarasov, L., Dyke, A. S., Adams, R. S., Allard, S., Atends, H. E., Atkinson, N., Attig, J. W., Barnett, P., Barnett, R., Batterson, M., Bernatchez, P., Borns, H. W., Breckenridge, A., Briner, J. P., Brouard, E., Campbell, J. E., Carlson, A. E.,..., Wright, H. E. (2020). An Updated Radiocarbon-Based Ice Margin Chronology for the Last Deglaciation of the North American Ice Sheet Complex. *Quaternary Science Reviews, 234*(15), 0277-3791. https://doi.org/10.1016/j.quascirev.2020.106223

Davis, P. T., Bierman, P. R., Marsella, K. A., Caffee, M. W., & Southon, J. (1999). Cosmogenic analysis of glacial terrains in the eastern Canadian Arctic: a test for inherited nuclides and the effectiveness of glacial erosion. *Annals of Glaciology*, *28*, 181–188. https://doi.org/10.3189/172756499781821805

Dunai, T. J., & Lifton, N. A. (2014). The nuts and bolts of cosmogenic nuclide production. *Elements*, *10*(5), 347–350. https://doi.org/10.2113/gselements.10.5.347

Dyke, A. S. (2004). An outline of North American deglaciation with emphasis on central and northern Canada. In *Developments in quaternary science* (pp. 373–424). https://doi.org/10.1016/s1571-0866(04)80209-4

Goehring, B. M., Kelly, M. A., Schaefer, J. M., Finkel, R. C., & Lowell, T. V. (2010). Dating of raised marine and lacustrine deposits in east Greenland using beryllium‐10 depth profiles and implications for estimates of subglacial erosion. *JQS. Journal of Quaternary Science/Journal of Quaternary Science*, *25*(6), 865–874. https://doi.org/10.1002/jqs.1380

Gosse, J. C., & Phillips, F. M. (2001). Terrestrial in situ cosmogenic nuclides: theory and application. *Quaternary Science Reviews*, *20*(14), 1475–1560. https://doi.org/10.1016/s0277-3791(00)00171-2

Gregoire, L., Ivanović, R., Maycock, A. C., Valdes, P. J., & Stevenson, S. (2018). Holocene lowering of the Laurentide ice sheet affects North Atlantic gyre circulation and climate. *Climate Dynamics*, *51*(9–10), 3797–3813. https://doi.org/10.1007/s00382-018-4111-9

Halsted, C. T., Bierman, P. R., Shakun, J. D., Davis, P. T., Corbett, L. B., Drebber, J. S., & Ridge, J. C. (2023). A critical re-analysis of constraints on the timing and rate of Laurentide Ice Sheet recession in the northeastern United States. *JQS. Journal of Quaternary Science/Journal of Quaternary Science*, *39*(1), 54–69. https://doi.org/10.1002/jqs.3563

Harbor, J. M., Stroeven, A. P., Fabel, D., Clarhäll, A., Klemån, J., Li, Y., Elmore, D., & Fink, D. (2006). Cosmogenic nuclide evidence for minimal erosion across two subglacial sliding boundaries of the late glacial Fennoscandian ice sheet. *Geomorphology*, *75*(1–2), 90–99. https://doi.org/10.1016/j.geomorph.2004.09.036

Hynes, A., & Rivers, T. (2010). Protracted continental collision — evidence from the Grenville OrogenThis article is one of a series of papers published in this Special Issue on the theme Lithoprobe — parameters, processes, and the evolution of a continent. *Canadian Journal of Earth Sciences*, *47*(5), 591–620. https://doi.org/10.1139/e10-003

Klein, J., Giegengack, R., Middleton, R., & Weeks, R. (1986). Revealing histories of exposure using insitu produced AL-26 and BE-10 in Libyan desert glass. *Radiocarbon*, *28*(547-555).

Kleman, J., Borgstrom, I., & Hattestrand, C. (1994). Evidence for a relict glacial landscape in Quebec-Labrador. Palaeogeography, Palaeoclimatology, Palaeoecology, 111(1994), 217-228.

Klemån, J., Jansson, K. N., De Angelis, H., Stroeven, A. P., Hättestrand, C., Alm, G., & Glasser, N. F. (2010). North American Ice Sheet build-up during the last glacial cycle, 115–21 kyr. *Quaternary Science Reviews*, *29*(17–18), 2036–2051. https://doi.org/10.1016/j.quascirev.2010.04.021

LeBlanc, D. E., Shakun, J. D., Corbett, L. B., Bierman, P. R., Caffe, M. W., & Hidy, A. J. (2023). Laurentide Ice Sheet Persistence During Pleistocene Interglacials. *Geology, 51*(5), 496-499. https://doi.org/10.1130/G50820.1

Larue, F., Royer, A., De Sève, D., Langlois, A., Roy, A., & Brucker, L. (2017). Validation of GlobSnow-2 snow water equivalent over Eastern Canada. *Remote Sensing of Environment*, *194*, 264–277. https://doi.org/10.1016/j.rse.2017.03.027

Margold, M., Stokes, C. R., & Clark, C. D. (2018). Reconciling records of ice streaming and ice margin retreat to produce a palaeogeographic reconstruction of the deglaciation of the Laurentide Ice Sheet. *Quaternary Science Reviews*, *189*, 1–30. https://doi.org/10.1016/j.quascirev.2018.03.013

Marsella, K. A., Bierman, P. R., Davis, P. T. and Caffee, M. W. (2000) Cosmogenic ^{10}Be and ^{26}Al ages for the last glacial maximum, eastern Baffin Island, Arctic Canada. *Geological Society of America Bulletin*. v. 112(8), p. 1296-1312. doi.org/10.1130/0016-7606(2000)112<1296:CBAAAF>2.0.CO;2

Marshall, S. J., Tarasov, L., Clarke, G. K. C., & Peltier, W. R. (2000). Glaciological reconstruction of the Laurentide Ice Sheet: physical processes and modelling challenges. *Canadian Journal of Earth Sciences*, *37*(5), 769–793. https://doi.org/10.1139/e99-113

Melanson, A., Bell, T., & Tarasov, L. (2013). Numerical modelling of subglacial erosion and sediment transport and its application to the North American ice sheets over the Last Glacial cycle. *Quaternary Science Reviews*, *68*, 154–174. https://doi.org/10.1016/j.quascirev.2013.02.017

Miller, G. H., & Andrews, J. T. (2019). Hudson Bay was not deglaciated during MIS-3. *Quaternary Science Reviews*, *225*, 105944. https://doi.org/10.1016/j.quascirev.2019.105944

Munroe, J. S., Perzan, Z., & Amidon, W. H. (2016). Cave sediments constrain the latest Pleistocene advance of the Laurentide Ice Sheet in the Champlain Valley, Vermont, USA. *JQS. Journal of Quaternary Science/Journal of Quaternary Science*, *31*(8), 893–904. https://doi.org/10.1002/jqs.2913

Nelson, A. H., Bierman, P. R., Shakun, J. D., & Hood, D. H. (2014). Using in situ cosmogenic 10Be to identify the source of sediment leaving Greenland. *Earth Surface Processes and Landforms, 39*, 1087-1100. 10.1002/esp.3565

Nishiizumi, K. (2004). Preparation of 26Al AMS standards. *Nuclear Instruments and Methods in Physics Research. Section B, Beam Interactions With Materials and Atoms/Nuclear Instruments & Methods in Physics Research. Section B, Beam Interactions With Materials and Atoms*, *223–224*, 388–392. https://doi.org/10.1016/j.nimb.2004.04.075

Nishiizumi, K., Kohl, C. P., Arnold, J. R., Klein, J., Fink, D., & Middleton, R. (1991). Cosmic ray produced 10Be and 26Al in Antarctic rocks: exposure and erosion history. *Earth and Planetary Science Letters*, *104*(2–4), 440–454. https://doi.org/10.1016/0012-821x(91)90221-3

Nishiizumi, K., Imamura, M., Caffee, M. W., Southon, J., Finkel, R. C., & McAninch, J. (2007). Absolute calibration of ^{10}Be AMS standards. *Nuclear Instruments and Methods in Physics Research. Section B, Beam Interactions With Materials and Atoms/Nuclear Instruments & Methods in Physics Research. Section B, Beam Interactions With Materials and Atoms*, *258*(2), 403–413. https://doi.org/10.1016/j.nimb.2007.01.297

Nishiizumi, K., Winterer, E. L., Kohl, C. P., Klein, J., Middleton, R., Lal, D., & Arnold, J. R. (1989). Cosmic ray production rates of 10Be and 26Al in quartz from glacially polished rocks. *Journal of Geophysical Research*, *94*(B12), 17907–17915. https://doi.org/10.1029/jb094ib12p17907

Payette, S., Morneau, C., Sirois, L., & Desponts, M. (1989). Recent fire history of the Northern Quebec

Biomes. *Ecology*, *70*(3), 656–673. https://doi.org/10.2307/1940217
Pico, T., Birch, L., Weisenberg, J., & Mitrovica, J. (2018). Refining the Laurentide Ice Sheet at Marine Isotope Stage 3: A data-based approach combining glacial isostatic simulations with a dynamic ice model. *Quaternary Science Reviews*, *195*, 171–179. https://doi.org/10.1016/j.quascirev.2018.07.023
Rasmussen, S. O., Andersen, K. H., Svensson, A., Steffensen, J. P., Vinther, B. M., Clausen, H., Siggaard-Andersen, M., Johnsen, S. J., Larsen, L. H., Dahl-Jensen, D., Bigler, M., Röthlisberger, R., Fischer, H., Goto-Azuma, K., Hansson, M., & Ruth, U. (2006). A new Greenland ice core chronology for the last glacial termination. *Journal of Geophysical Research*, *111*(D6). https://doi.org/10.1029/2005jd006079
Rivers of Canada - Churchill River : Can Geo Education. (n.d.). https://web.archive.org/web/20200201124628/http://www.cangeoeducation.ca/resources/rivers_of_canada/churchill_river/default.asp
Roy, M., Hemming, S. R., & Parent, M. (2009). Sediment sources of northern Québec and Labrador glacial deposits and the northeastern sector of the Laurentide Ice Sheet during ice-rafting events of the last glacial cycle. *Quaternary Science Reviews*, *28*(27–28), 3236–3245. https://doi.org/10.1016/j.quascirev.2009.08.008
Spray, J. G., Kelley, S. P., & Rowley, D. B. (1998). Evidence for a late Triassic multiple impact event on Earth. *Nature*, *392*(6672), 171–173. https://doi.org/10.1038/32397
Staiger, J. K. W., Gosse, J. C., Johnson, J. V., Fastook, J. L., Gray, J., Stöckli, D. F., Stockli, L. D., & Finkel, R. C. (2005). Quaternary relief generation by polythermal glacier ice. *Earth Surface Processes and Landforms*, *30*(9), 1145–1159. https://doi.org/10.1002/esp.1267
Staiger, J. W., Marchant, D. R., Schaefer, J. M., Oberholzer, P., Johnson, J. V., Lewis, A. R., & Swanger, K. M. (2006). Plio-Pleistocene history of Ferrar Glacier, Antarctica: Implications for climate and ice sheet stability. *Earth and Planetary Science Letters*, *243*(3–4), 489–503. https://doi.org/10.1016/j.epsl.2006.01.037
Stokes, C. R., Tarasov, L., & Dyke, A. S. (2012). Dynamics of the North American Ice Sheet Complex during its inception and build-up to the Last Glacial Maximum. *Quaternary Science Reviews*, *50*, 86–104. https://doi.org/10.1016/j.quascirev.2012.07.009
Stroeven, A. P., Fabel, D., Hättestrand, C., & Harbor, J. M. (2002). A relict landscape in the centre of Fennoscandian glaciation: cosmogenic radionuclide evidence of tors preserved through multiple glacial cycles. *Geomorphology*, *44*(1–2), 145–154. https://doi.org/10.1016/s0169-555x(01)00150-7
Süfke, F., Gutjahr, M., Keigwin, L. D., Reilly, B. T., Giosan, L., & Lippold, J. (2022). Arctic drainage of Laurentide Ice Sheet meltwater throughout the past 14,700 years. *Communications Earth & Environment*, *3*(1). https://doi.org/10.1038/s43247-022-00428-3
Tarasov, L., Dyke, A. S., Neal, R. M., & Peltier, W. R. (2012). A data-calibrated distribution of deglacial chronologies for the North American ice complex from glaciological modeling. *Earth and Planetary Science Letters*, *315–316*, 30–40. https://doi.org/10.1016/j.epsl.2011.09.010
Ullman, D. (2023). The retreat chronology of the Laurentide Ice Sheet during the last 10,000 years and implications for deglacial sea-level rise. *Vignettes: Key Concepts in Geomorphology.* https://serc.carleton.edu/59463.
Ullman, D., Carlson, A. E., Hostetler, S. W., Clark, P. U., Cuzzone, J., Milne, G. A., Windsor, K., & Caffe, M. (2016). Final Laurentide ice-sheet deglaciation and Holocene climate-sea level change. *Quaternary Science Reviews, 152*(15), 49.59. https://doi.org/10.1016/j.quascirev.2016.09.014

Appendix. Field Sample Notes

~~**GB-01**~~

Sample Type: Modern river sediment
Collection Date: 07/30/2022
Relative Location: Sandbar from Churchill River
Absolute Location: 53° 17’ 17.0’’ N, 60° 19’ 23.8’’ W
Elevation: 0 feet
Description/Notes: The sample was taken across the river from a sandbar, preventing close up pictures being taken of the sample site. Jeremy had to walk through the river to reach the sand bar (luckily the water was relatively shallow). Sample was mostly fine sand with some silt. Vegetation was about 50 meters away from the sample site.

GB-02

Sample Type: Modern river sediment
Collection Date: 07/30/2022
Relative Location: Large point bar on the interior section of the Goose River. 80 meters away from an unnamed bridge.
Absolute Location: 53° 23’ 36.3’’ N, 60° 25’ 22.6’’ W
Elevation: 5 feet
Description/Notes: Sample was composed of coarse sand taken right on the water line from a point bar about 10 m across from a cut bank. The cut bank showcased a 30m high sediment sequence, which we assumed to be deglacial. Sample site was 30m from vegetation. *Extreme* off trail bushwhacking was needed in order to reach the sand bar.

GB-03

Sample Type: Deglacial sediment
Collection Date: 07/30/2022
Relative Location: Adjacent to Muskrat Dam parking area and human altered boulders and cobbles. In Churchill River Valley.
Absolute Location: 53° 15’ 26.14’’ N, 60° 18’ 48.5’’ W
Elevation: 36 meters
Description/Notes: Sample is coarse, medium sand taken from 1m above the water level at the Churchill River. We dug about a foot into the sediment for collection. Sediment was part of a very large glaciofluvial delta filling in most of the Churchill River Valley.

GB-04

Sample Type: Modern stream sediment
Collection Date: 07/30/2022
Relative Location: Tributary to Churchill River.
Absolute Location: 53° 13' 12.25" N, 60° 57' 17.53" W
Elevation: 210 feet
Description/Notes: We were unsure if this sample spot was *entirely* upstream of the lower churchill river valley glaciofluvial delta fill. We took the sample interested to see upon analysis if it was truly a modern sediment sample or simply reworked deglacial sediment. It was difficult to sort out cobbles during sample collection.

GB-05

Sample Type: Glacial sediment/esker
Collection Date: 07/30/2022
Relative Location: Adjacent to anthropogenic gravel pit.
Absolute Location: 53° 5' 31.96" N, 61° 53' 31.02" W
Elevation: 402 meters
Description/Notes: The sample was taken from an exposed slope of the esker that was about 6m high. Collection occurred 1m from the base of the slope and the sample was predominantly coarse sand and cobbles. We took special note that the slope looked in situ and undisturbed by the nearby gravel mining. This sample site was suggested to us by Pierre Olivier.

GB-06

Sample Type: Bedrock
Collection Date: 07/30/2022
Relative Location: A knoll on the south side of the Trans-Labrador Highway.
Absolute Location: 53° 20' 6.25" N, 62° 59' 28.14" W
Elevation: 484 meters
Description/Notes: The rock's highest point is about 2m from the surrounding ground. The rock was crystalline and possibly granite. Strike and dip was not measured. However, a 10° slight dip away from the highway was estimated. There was no topographic shielding.

CF-01

Sample Type: Modern river sediment
Collection Date: 07/31/2022
Relative Location: The base of a 100 m slope adjacent to the water. Facing upriver, the sample site was to the right of us.
Absolute Location: 53° 30' 21.564" N, 63° 57' 30.672" W
Elevation: 126 meters
Description/Notes: This was the most isolated sampling location of the whole excursion. It took us 40 minutes to descend a narrow, steep valley in order to reach a remote river bank. Collection took place near a deglacial sediment sequence. However, since we were about 100 m upstream of this area, we concluded that it is safe to assume the sample is modern with no contribution coming from deglacial debris. Sample site was also near vegetation. Before collection, the sample was wet sieved between 250-1000 microns. There were multiple cases of exceptional sampling sites being inaccessible during the ascent back up the valley to the van. We could see areas with clear stratigraphy and were disappointed that they were out of reach due to near vertical angles.

CF-02

Sample Type: Deglacial sediment
Collection Date: 07/31/2022
Relative Location: About 0.5 m below the surface of a ridge on the ascent back to the van from CF-01 sample collection.
Absolute Location: 53° 30' 27.72" N, 63° 57' 16.272" W
Elevation: 167 meters
Description/Notes: Sample site was horizontally bedded and appeared to have slumped down a bit from the top of the ridge. The top layer consisted of soil/mud (about 10 cm) before progressing to coarser sand further down. According to information from Pierre, this landscape is part of a deglacial delta.

~~**CF-03**~~

Sample Type: Modern river sediment
Collection Date: 07/31/2022
Relative Location: Bank of unknown river on the west side of an unpaved road south of the Trans-Labrador Highway.
Absolute Location: 53° 34' 53.868" N, 64° 30' 20.052" W
Elevation: 416 meters
Description/Notes: Sample made up of very coarse sand with intermixed large cobbles. Wet sieving between 250-1000 microns was used. Collection site was less than 1 meter from dense riverbank vegetation and was downstream from a dam.

~~**CF-04**~~

Sample Type: Bedrock
Collection Date: 07/31/2022
Relative Location: Bedrock mass visible from roadside. About a 20 minute hike from the road to the sample site.
Absolute Location: 53° 20' 26.9154" N, 65° 41' 44.9514" W
Elevation: 602 meters
Description/Notes: Sample taken from a knob of bedrock rising about 5 m above the surrounding terrain. Less than 5° of topographic shielding. Strike was 305° and dip was 4° northeast.

CF-05

Sample Type: Modern river sediment
Collection Date: 07/31/2022
Relative Location: The south shore of the Ashuanipi River. There was a nearby construction site (about 50m away). But, it was not close enough to make us believe the sediment could have been intermingled with construction tailings.
Absolute Location: 53° 3' 34.1634" N, 66° 15' 19.836" W
Elevation: 527 meters
Description/Notes: There were a fair amount of cobbles and pebbles were mixed in with our sand sample. We also were not able to find a clear sediment source to the river. This river also had a very fast flow.

LC-01

Sample Type: Modern river sediment
Collection Date: 08/01/2022
Relative Location: The shore of the Riviere Peppler. We sampled about 50 m upstream of a bridge where a road crosses the river.
Absolute Location: 52° 20' 11.2194" N, 67° 34’ 1.632’’ W
Elevation: 533 meters
Description/Notes: This river had relatively slow flow and was nearby to a few cottages and a dirt road. We sampled believing that there was little to no risk that the road and houses contributed sediment to the sample site.

LC-02

Sample Type: Esker
Collection Date: 08/01/2022
Relative Location: Sample site right next to Petite Riviere Manicouagan. Sample was taken 4 meters above a lake surface and 3 meters below the top of the sediment deposit.
Absolute Location: 52° 12' 3.924" N, 67° 52' 19.9914" W
Elevation: 537 meters
Description/Notes: The sample was taken from a 10 m high sediment exposure. The esker/deposit is predominantly medium sand that is stratified with wavy/rippled layers. There was nearby vegetation. This location was suggested to us by Pierre Olivier.

LC-03

Sample Type: Modern river sediment
Collection Date: 08/01/2022
Relative Location: Sample taken from a sandy creek right off of the highway (less than 10 minute walk from the road).
Absolute Location: 52° 6' 38.376" N, 68° 0' 26.352" W
Elevation: 645 meters
Description/Notes: We sampled about 20 meters upstream of where the road comes closest to the water. As you can see in the photo, the water had a heavy red tint. We also wet sieved on site between 250-1000 micrometers (also shown in photo).

LC-04

Sample Type: Deglacial deposit
Collection Date: 08/01/2022
Relative Location: Sample taken from a deglacial deposit exposed in a gravel quarry.
Absolute Location: 51° 42' 36.6834" N, 68° 4' 18.7674" W
Elevation: 440 meters
Description/Notes: The exposure was 15 meters high with wavy, stratified fine sand layers at the top and more coarse sand layers near the bottom. The fine sand layers hosted large, floating dropstones. We sampled the contact between both layers. This site was tipped off to us as an ice contact deposit by Pierre Olivier.

LC-05

Sample Type: Glacial outwash
Collection Date: 08/01/2022
Relative Location: Sample taken from a gravel pit.
Absolute Location: 51° 29' 17.304" N, 68° 13' 9.012" W
Elevation: 391 meters
Description/Notes: We sampled halfway up a 10 meter high exposure. Boulders and cobbles at this site were very loose so we only sent one person up to take the sample while the rest of us stood away from the edge of the exposure for safety. We were all apprehensive if a worker from the gravel pit was going to question why we were there.

LC-06

Sample Type: Modern stream sediment
Collection Date: 08/01/2022
Relative Location: Sample taken from a stream very near to the gravel pit from sample site LC-05. The stream was adjacent to the road, so we sampled 15 meters upstream of the road.
Absolute Location: 51° 29' 17.376" N, 68° 13' 22.512" W
Elevation: 401 meters
Description/Notes: We decided to take the sample because it appeared that no gravel pit sediments or road sediments had traveled into the stream.

MC-01

Sample Type: Deglacial sediment
Collection Date: 08/02/2022
Relative Location: Sample taken from a glaciofluvial deposit/outwash esker in a gravel pit.
Absolute Location: 50° 28' 29.3874" N, 68° 48' 36.2154" W
Elevation: 500 meters
Description/Notes: Sample site had beautiful wavy/rippled laminated sediments. We dig into the deposit about 1.8 meters below the surface of the exposure.

MC-02

Sample Type: Deglacial sediment
Collection Date: 08/02/2022
Relative Location: Pointe-des-Fortin beach on the north shore of the Saint Lawrence River.
Absolute Location: 48° 38' 42.648" N, 69° 5' 7.5114" W
Elevation: 10 meters
Description/Notes: Sampled the bottom of sandy forest beds in the deglacial delta along the beach. We sampled 1 meter above the contact. Sediment below the contact had increasingly more clay.

MC-03

Sample Type: Modern river sediment
Collection Date: 08/02/2022
Relative Location: 15 km upstream of Pointe-des-Fortin.
Absolute Location: 48° 40' 40.5834" N, 69° 18' 16.0914" W
Elevation: 61 meters
Description/Notes: The riverbanks here were 10-20 meter high stratified sediment sequences. The sequences were composed of gray clay and sand. We assumed that the sediments were part of the same deglacial delta as MC-02. We considered that some or most of the “modern” river sediment in our sample are just remobilized deglacial sediment from the last site.

SS-01

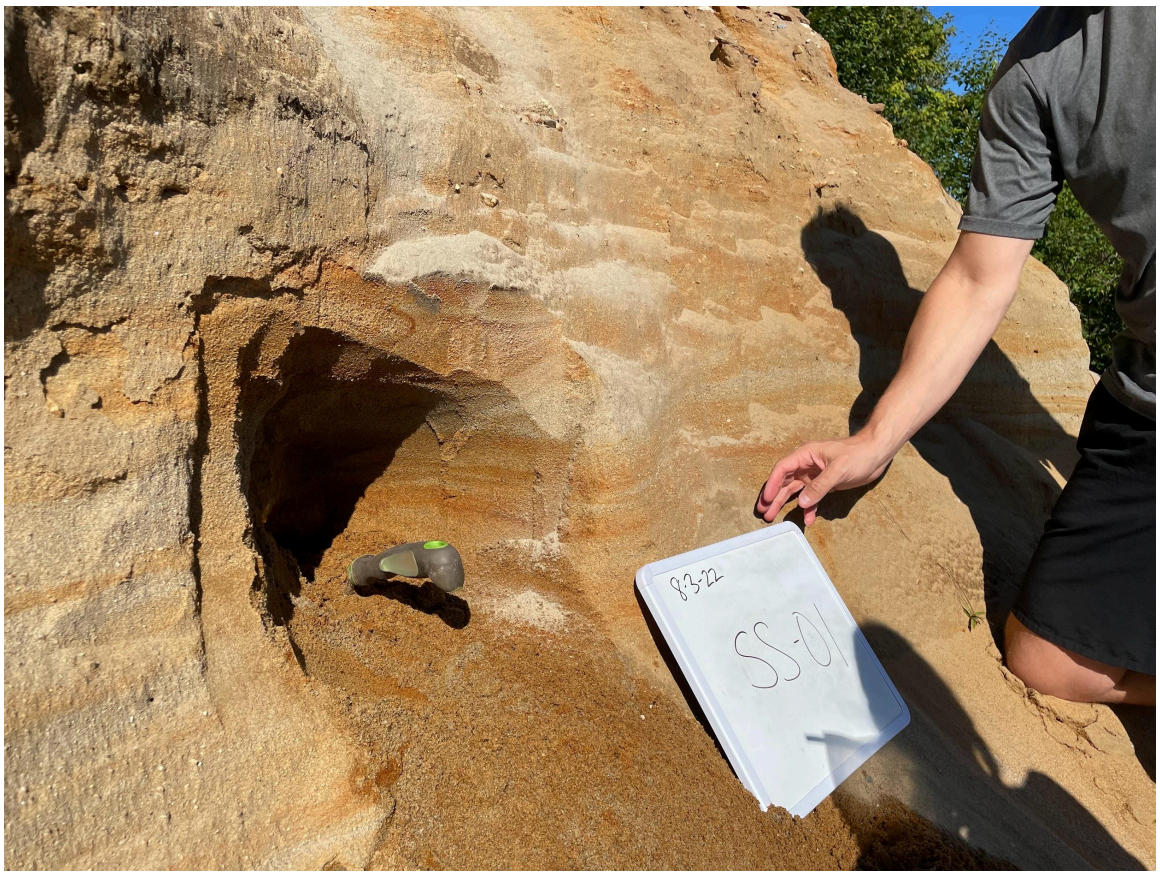

Sample Type: Deglacial sediment
Collection Date: 08/03/2022
Relative Location: Baie St. Catherine
Absolute Location: 48° 6' 10.872" N, 69° 43' 16.6074" W
Elevation: 10 meters
Description/Notes: The deglacial delta we sampled from was near sandy forests and was 1.5 meters above the beach. The bluff was about 15 meters. Digging into the bluff revealed wavy/rippled stratigraphy with some very red sediment layers.

SS-02

Sample Type: Modern creek sediment
Collection Date: 08/03/2022
Relative Location: 7 km upriver from Saint Simeon and 15 meters from the side of the highway. Sample site was well inland of the Saint Lawrence river.
Absolute Location: 47° 53' 39.1914" N, 69° 56' 12.3714" W
Elevation: 128 meters
Description/Notes: We collected the sample from a sand/gravel bar on the side of the river. We were a few meters upriver from a confluence with a side drainage coming under the highway. Because of the rugged topography and being well inland of the St. Lawrence, we figured it was safe to assume that this river's sediments are dominated by modern inland input.

SS-03

Sample Type: Modern creek sediment
Collection Date: 08/03/2022
Relative Location: Next to the highway in the town of La Malbaie. The sample site was behind a family campsite area.
Absolute Location: 47° 39' 59.508" N, 70° 9' 32.184" W
Elevation: 3 meters
Description/Notes: Sample came from a large gravel bar. We had to dig away the top layer of large cobbles with our hands to reveal wet sand underneath. It was difficult to scoop the sample while avoiding collecting too many cobbles. The sample also had a very strong, fishy odor.

SS-04

Sample Type: Modern creek sediment
Collection Date: 08/03/2022
Relative Location: Sandy point bar along Gouffre River (tributary of St. Lawrence River).
Absolute Location: 47° 30' 56.6274" N, 70° 30' 23.58" W
Elevation: 25 meters
Description/Notes: We wet sieved the sample between 250-1000 micrometers. Vegetation was about 5 meters from the sample site. Sample was mostly medium to coarse sand with some intermingled pebbles.

SS-05

Sample Type: Deglacial sediment
Collection Date: 08/03/2022
Relative Location: A quarry in the St. Leon delta.
Absolute Location: 47° 10' 0.6954" N, 70° 48' 16.7754" W
Elevation: 307 meters
Description/Notes: We sampled 3 meters from the base of the bluff. There were 100 meters of stratigraphy at the top of the sample site. Layers were mixed in with large cobbles and pebbles below the sample point.